

Energy-conserving explicit and implicit time integration methods for the multi-dimensional Hermite-DG discretization of the Vlasov-Maxwell equations

C. Pagliantini^{*}, G. Manzini[†], O. Koshkarov[‡], G. L. Delzanno[§], and V. Roytershteyn[¶]

Abstract

We study the conservation properties of the Hermite-discontinuous Galerkin (Hermite-DG) approximation of the Vlasov-Maxwell equations. In this semi-discrete formulation, the total mass is preserved independently for every plasma species. Further, an energy invariant exists if central numerical fluxes are used in the DG approximation of Maxwell's equations, while a dissipative term is present when upwind fluxes are employed. In general, traditional temporal integrators might fail to preserve invariants associated with conservation laws during the time evolution. Hence, we analyze the capability of explicit and implicit Runge-Kutta (RK) temporal integrators to preserve such invariants. Since explicit RK methods can only ensure preservation of linear invariants but do not provide any control on the system energy, we consider modified explicit RK methods in the family of relaxation Runge-Kutta methods (RRK). These methods can be tuned to preserve the energy invariant at the continuous or semi-discrete level, a distinction that is important when upwind fluxes are used in the discretization of Maxwell's equations since upwind provides a numerical source of energy dissipation that is not present when central fluxes are used. We prove that the proposed methods are able to preserve the energy invariant and to maintain the semi-discrete energy dissipation (if present) according to the discretization of Maxwell's equations. An extensive set of numerical experiments corroborates the theoretical findings. It also suggests that maintaining the semi-discrete energy dissipation when upwind fluxes are used leads to an overall better accuracy of the method relative to using upwind fluxes while forcing exact energy conservation.

Keyword. 3-D Vlasov-Maxwell equations, Conservation laws, Runge-Kutta temporal integrators, Hermite-Discontinuous Galerkin discretization

1 Introduction

The Vlasov-Maxwell equations for modeling collisionless plasmas in presence of self-consistent electromagnetic fields possess an infinite number of invariants, i.e., quantities that do not change while the physical system evolves in time [1, 3, 15]. These quantities are related to the moments of the particle distribution functions with respect to the independent velocity variable and include terms in their definition that may depend on the electromagnetic fields. Importantly, a few of them express fundamental properties of the physical system such as the conservation of the number of particles, which also entails mass and charge conservation, the conservation of the total momentum and the conservation of the total energy.

^{*} *Corresponding author.* Centre for Analysis, Scientific computing and Applications, Eindhoven University of Technology, 5600 MB Eindhoven, The Netherlands. Email: c.pagliantini@tue.nl

[†]T-5 Applied Mathematics and Plasma Physics Group, Los Alamos National Laboratory, Los Alamos, NM 87545, USA. Email: gmanzini@lanl.gov

[‡]T-5 Applied Mathematics and Plasma Physics Group, Los Alamos National Laboratory, Los Alamos, NM 87545, USA. Email: koshkarov@lanl.gov

[§]T-5 Applied Mathematics and Plasma Physics Group, Los Alamos National Laboratory, Los Alamos, NM 87545, USA. Email: delzanno@lanl.gov

[¶]Space Science Institute, 4765 Walnut St, Suite B, Boulder, CO 80301, USA. Email: vroytershteyn@spacescience.org

Reproducing some (or all) of the conservation properties mentioned above in the discrete setting makes a numerical method very compelling, but at the same time it is a nontrivial task [26]. Indeed, it turns out that for only very few numerical methods we can define discrete invariants that can be calculated from the numerical solution and correspond to the number of particles, the total momentum or the total energy of the physical model.

The majority of the literature on numerical schemes able to preserve key invariants of motion at the fully discrete level has focused on particle-based discretizations. Variational algorithms were introduced in [11, 32, 33] based on least action principles. Energy-conserving time integrators for finite element particle-in-cell discretizations of the Vlasov–Maxwell equations have been recently proposed in [5, 28]. Using the Hamiltonian formulation of some kinetic plasma models, Refs. [22, 30, 39] have focused on the preservation of the phase-space structure, via e.g. symplectic integrators, while ensuring global bounds of the numerical errors of conserved quantities.

In a series of previous works [10, 29, 34], it was shown that the spectral expansion of the plasma distribution function, see also [38], makes it possible to formulate numerical methods for the solution of the kinetic equations that show excellent conservation properties and posses many other desirable properties. Such methods are particularly attractive for problems that involve fluid-kinetic coupling, i.e., the coupling between macroscopic and microscale system dynamics. That is because a suitable choice of the spectral basis makes the fluid-kinetic coupling an intrinsic property of the numerical approximation: the low-order terms of the expansion provide a fluid description of the plasma while additional higher-order terms are able to capture features from the underlying kinetics.

In the present work, we investigate the conservation properties for one such method: the numerical approximation of the system of Vlasov-Maxwell equations provided by the spectral-discontinuous Galerkin method proposed in [29]. The method is based on a spectral expansion in velocity space using asymmetrically-weighted Hermite basis functions and an approximation in physical space using piecewise discontinuous polynomials of a given order. The discontinuous Galerkin (DG) method is also applied to the discretization in space of the time-dependent Maxwell equations. Unlike the work presented in [29], here we treat the fully discrete case and focus on the conservation of the total number of particles and the total energy of the system.

The conservation of the number of particles, which implies mass and charge conservation, is a consequence of the conservative formulation of the method, and holds regardless of the discontinuity of the approximate solution fields. However, the discontinuous nature of the approximate distribution functions and electromagnetic fields plays a major role in the conservation of the total momentum and the total energy. Indeed, the momentum is not conserved and a dissipative term proportional to the square of the jumps of the electromagnetics fields affects the energy conservation when upwind numerical fluxes are used in the discretization of Maxwell’s equations. The total energy is instead conserved when central numerical fluxes are adopted for Maxwell’s equations.

We remark that the work of Ref. [29] does not deal with temporal integration. On the contrary, the present manuscript studies the numerical temporal discretization of the system of ordinary differential equations resulting from the aforementioned DG-Hermite discretization. In particular, we study the effect of time integration on the conservation of mass and energy, i.e., the invariants of the semi-discrete problem. The availability of time discretizations able to satisfy the conservation laws of the continuous or semi-discrete problem is of fundamental importance to ensure numerical solutions that reproduce key physical properties of kinetic models. With this objective in mind, we consider two families of one-step temporal integrators: explicit Runge-Kutta methods and (implicit) Gauss-Legendre methods. First, we show that the implicit Gauss-Legendre schemes are able to preserve both the conserved quantities and the dissipation of the total energy, meaning that the amount of energy dissipated by the fully-discrete scheme equals the temporal approximation of the dissipative term ensuing from the Hermite-DG semi-discrete formulation. Secondly, we study the properties of explicit RK schemes: they ensure the preservation of the number of particles (linear invariant) but do not guarantee any control on the evolution of the total energy. However, in practical implementation of plasma solvers, the explicit schemes are often preferred to the implicit ones despite the superior stability and conservation properties of the latter. The reason is that explicit schemes are computationally cheap, unlike implicit schemes whose computational cost is dominated by the solution of a nonlinear system of equations at each time step. This remark also

suggests that the availability of *explicit* RK methods of arbitrary order able to preserve the conservation and dissipation laws of the continuous or semi-discrete problem could have a significant impact on the efficient solution of kinetic plasma models. We address this issue by resorting to explicit RK methods based on projection. Projection methods, *cf.* for instance [12, Section 5.3] and [18], belong to the class of extrinsic numerical time integrators and are based on the projection of the numerical solution onto the manifold that is constrained by a given conservation property. The projection methods considered in this work consist in modifying the RK step by suitable scalar factors that depend on the approximate solution and are determined by the given conservation/dissipation law. This approach was originally proposed in [8, pp. 265–266] to derive conservative RK methods. The idea was extended in [9] to a restricted class of fourth-order methods and further developed in [4] via the so-called incremental direction technique (IDT). More recently, an extension of these methods to preserve inner-product norms of the solution has led to the so-called relaxation Runge–Kutta (RRK) methods [27]. We analyze this family of modified RK methods in the context of the Hermite-DG discretization of the Vlasov-Maxwell equations. For the semi-discrete problem considered, this correction guarantees the preservation of the energy invariant and can be tuned to preserve it either at the continuous level, or at the semi-discrete level (this distinction is only relevant when upwind numerical fluxes are used in Maxwell’s equations, since for central fluxes the total energy is conserved at both continuum and semi-discrete levels). With numerical experiments, we show that the latter choice that maintains the semi-discrete energy dissipation when upwind numerical fluxes are used in the discretization of Maxwell’s equations leads to a better overall accuracy of the method relative to a method that uses upwind fluxes but forces exact energy conservation.

The remainder of the paper is organized as follows. In Section 2, we introduce the Vlasov-Maxwell equations as the mathematical model that describes the transport phenomena of different charged particle species in a collisionless plasma under the action of the self-consistent electromagnetic field. Section 3 is devoted to the temporal discretization of the Vlasov-Maxwell equations by using explicit Runge-Kutta methods and implicit Gauss-Legendre methods that are reformulated as a single time-evolution problem. In Section 4, we summarize the space-velocity discretization of the Vlasov-Maxwell equations performed with the Hermite-DG methods introduced in [29]. Next, Section 5 pertains to the study of the conservation laws associated with the total number of particles and the total energy and to their characterization as conserved quantities of the ODE resulting from the semi-discrete system of Vlasov-Maxwell equations. In Section 6, we analyze the capability of Runge-Kutta temporal integrators to preserve the conservative and dissipative relations associated with the different spatial discretizations, and we study modified explicit schemes that preserve mass and total energy of the semi-discrete Vlasov-Maxwell problem. In Section 7, we experimentally assess the performance of the proposed methods on the whistler instability test case, on the Orzsag-Tang vortex test case, and in resolving dispersion properties of high frequency waves. Finally, in Section 8 we present some conclusions and final considerations.

Notation and normalization. We normalize the model equations as follows. Time t is normalized to the electron plasma frequency $\omega_{pe} = \sqrt{e^2 n_0^e / \varepsilon_0 m^e}$, where e is the elementary charge, m^e is the electron mass, ε_0 is the permittivity of vacuum, and n_0^e is a reference electron density. The velocity coordinate v is normalized to the speed of light c ; the spatial coordinate x is normalized to the electron inertial length $d_e = c/\omega_{pe}$; the magnetic field \mathbf{B} is normalized to a reference magnetic field \mathcal{B}_0 , and the electric field is normalized to $c\mathcal{B}_0$. We denote the quantities associated with a given plasma species by the superscript s , which may take the specific values $s = e$ (electrons) and $s = i$ (ions), etc. Accordingly, we denote the mass of the particles of species s by m^s and their charge by $q^s = \pm e$. We normalize the charge q^s and the mass m^s to the elementary charge e and the mass m^e , respectively. Finally, we define the cyclotron frequency of species s as $\omega_{cs} = e\mathcal{B}_0/m^s$. For simplicity, we maintain the same symbol for each normalized variable and from now on we will only consider normalized quantities.

2 Vlasov-Maxwell equations

The Vlasov-Maxwell equations provide a model for collisionless plasmas [16]. At any time instant $t > 0$, the behavior of the particles of species s in the plasma is described by the non-negative distribution function $f^s(\mathbf{x}, \mathbf{v}, t)$, where \mathbf{x} denotes the position in the physical space Ω_x and \mathbf{v} the position in the velocity space Ω_v . The plasma evolves self-consistently under the action of the electric and magnetic

fields $\mathbf{E}(\mathbf{x}, t)$ and $\mathbf{B}(\mathbf{x}, t)$ generated by particles' motion (and external sources): the distribution function of species s satisfies the (normalized) Vlasov equation

$$\frac{\partial f^s}{\partial t} + \mathbf{v} \cdot \nabla_{\mathbf{x}} f^s + \frac{q^s}{m^s} \frac{\omega_{ce}}{\omega_{pe}} (\mathbf{E} + \mathbf{v} \times \mathbf{B}) \cdot \nabla_{\mathbf{v}} f^s = 0. \quad (1)$$

Let \mathbf{J} and ρ denote the self-consistent electric current and charge density, respectively, induced by the plasma particles, namely

$$\rho(\mathbf{x}, t) = \sum_{s=1}^{N_s} q^s \int_{\Omega_v} f^s(\mathbf{x}, \mathbf{v}, t) d\mathbf{v}, \quad \mathbf{J}(\mathbf{x}, t) = \sum_{s=1}^{N_s} q^s \int_{\Omega_v} \mathbf{v} f^s(\mathbf{x}, \mathbf{v}, t) d\mathbf{v},$$

where N_s denotes the number of plasma species. The electric and magnetic fields \mathbf{E} and \mathbf{B} satisfy the time-dependent wave propagation equations

$$\frac{\partial \mathbf{E}}{\partial t} - \nabla_{\mathbf{x}} \times \mathbf{B} = -\frac{\omega_{pe}}{\omega_{ce}} \mathbf{J}, \quad (2)$$

$$\frac{\partial \mathbf{B}}{\partial t} + \nabla_{\mathbf{x}} \times \mathbf{E} = 0, \quad (3)$$

and the divergence equations

$$\nabla_{\mathbf{x}} \cdot \mathbf{E} = \frac{\omega_{pe}}{\omega_{ce}} \rho,$$

$$\nabla_{\mathbf{x}} \cdot \mathbf{B} = 0.$$

We consider the unbounded velocity space $\Omega_v = \mathbb{R}^3$ and we assume that, for $|\mathbf{v}| \rightarrow \infty$, each distribution function f^s decays sufficiently fast, e.g. as $\exp(-|\mathbf{v}|^2)$ [15]. For example, this assumption is physically consistent with near-Maxwellian velocity distribution of a plasma close to thermodynamic equilibrium [17]. Similarly, we consider the closed bounded subset $\Omega_x \subset \mathbb{R}^3$ with boundary $\partial\Omega_x$, and we assume that suitable problem-dependent boundary conditions for f^s , \mathbf{E} , and \mathbf{B} are prescribed at $\partial\Omega_x$ for any time t and any \mathbf{v} in Ω_v . Moreover, we consider the plasma evolution in the temporal interval $[0, T]$ and assume that physically meaningful initial conditions are provided for the unknown fields f^s , \mathbf{E} , \mathbf{B} at the initial time $t = 0$. Since we pursue a numerical approximation of the Vlasov-Maxwell equations based on a spatial discontinuous Galerkin method, we reformulate Eqs. (2)-(3) in conservative form as follows. Let us introduce, for any $t > 0$ and $\mathbf{x} \in \Omega_x$, the vector of conservative unknowns \mathbf{u} and the source term \mathbf{S} ,

$$\mathbf{u}(\mathbf{x}, t) := \begin{pmatrix} \mathbf{E}(\mathbf{x}, t) \\ \mathbf{B}(\mathbf{x}, t) \end{pmatrix}, \quad \mathbf{S}(\mathbf{x}, t) = \begin{pmatrix} \mathbf{S}_{\mathbf{E}} \\ \mathbf{S}_{\mathbf{B}} \end{pmatrix} := -\frac{\omega_{pe}}{\omega_{ce}} \begin{pmatrix} \mathbf{J}(\mathbf{x}, t) \\ \mathbf{0} \end{pmatrix}, \quad (4)$$

and the fluxes,

$$\mathbb{F}(\mathbf{u}) := \begin{pmatrix} \mathbb{F}_{\mathbf{E}}(\mathbf{u}) \\ \mathbb{F}_{\mathbf{B}}(\mathbf{u}) \end{pmatrix}, \quad \nabla_{\mathbf{x}} \cdot \mathbb{F}(\mathbf{u}) = \begin{pmatrix} \nabla_{\mathbf{x}} \cdot \mathbb{F}_{\mathbf{E}}(\mathbf{u}) \\ \nabla_{\mathbf{x}} \cdot \mathbb{F}_{\mathbf{B}}(\mathbf{u}) \end{pmatrix} = \begin{pmatrix} -\nabla_{\mathbf{x}} \times \mathbf{B} \\ \nabla_{\mathbf{x}} \times \mathbf{E} \end{pmatrix}, \quad (5)$$

where the operator $\nabla_{\mathbf{x}} \cdot$ denotes here the row-wise divergence in physical space. An explicit form for fluxes \mathbb{F} is given in Section 4.1. With these definitions, Maxwell's equations (2) and (3) can be written in conservative form as

$$\frac{\partial \mathbf{u}}{\partial t} + \nabla_{\mathbf{x}} \cdot \mathbb{F}(\mathbf{u}) = \mathbf{S}(\mathbf{x}, t). \quad (6)$$

3 Temporal discretization of the Vlasov-Maxwell equations

For the numerical approximation of the Vlasov-Maxwell equations, we pursue a method of line approach with Runge-Kutta temporal integrators coupled with the DG-spectral approximation in space-velocity introduced in [29], and summarized in Section 4.

Since the focus of this work is on numerical time integrators, we start by reformulating the Vlasov equation (1) for every plasma species s , and the wave propagation equations (2)-(3) as a single time-evolution problem and consider its temporal discretization. To this aim, consider the vector-valued function collecting all the unknowns

$$\mathbf{Y}(\mathbf{x}, \mathbf{v}, t) = \begin{pmatrix} (f^s(\mathbf{x}, \mathbf{v}, t))_s \\ \mathbf{E}(\mathbf{x}, t) \\ \mathbf{B}(\mathbf{x}, t) \end{pmatrix}, \quad t > 0, \mathbf{x} \in \Omega_x, \mathbf{v} \in \Omega_v, s = 1, \dots, N_s. \quad (7)$$

The function \mathbf{Y} satisfies the partial differential equation

$$\frac{\partial \mathbf{Y}}{\partial t} = \mathcal{F}(\mathbf{Y}; \mathbf{x}, \mathbf{v}, t) \quad \text{in } \Omega_x \times \Omega_v \times (0, T], \quad (8)$$

with suitable initial conditions $\mathbf{Y}(\mathbf{x}, \mathbf{v}, 0) = \mathbf{Y}_0(\mathbf{x}, \mathbf{v})$, and boundary conditions, as described in Section 2. The operator \mathcal{F} in (8) is defined as

$$\mathcal{F}(\mathbf{Y}; \mathbf{x}, \mathbf{v}, t) = \begin{pmatrix} (-\mathbf{v} \cdot \nabla_{\mathbf{x}} f^s - \frac{q^s}{m^s} \frac{\omega_{ce}}{\omega_{pe}} (\mathbf{E} + \mathbf{v} \times \mathbf{B}) \cdot \nabla_{\mathbf{v}} f^s)_s \\ \mathbf{S}(\mathbf{x}, t) - \nabla_{\mathbf{x}} \cdot \mathbb{F}(\mathbf{u}) \end{pmatrix}, \quad (9)$$

where the first term corresponds to the Vlasov equation (1), while the second term is associated with Maxwell's equations in conservative form (6). The boundary conditions can be introduced in the above setting through additional conditions on the unknown functions f^s and \mathbf{u} or by suitably including them in the discretization in space and velocity that is introduced in Section 4.

For the temporal discretization of problem (8), we split the time integration domain $(0, T]$ into the union of intervals $(t^\tau, t^{\tau+1}]$, $\tau \in \mathbb{N}_0$, with time step $\Delta t^\tau = t^{\tau+1} - t^\tau$. Let us denote by $\mathbf{Y}^\tau(\mathbf{x}, \mathbf{v})$ the approximation of the function (7) at time t^τ , and assume that the initial condition $\mathbf{Y}^0(\mathbf{x}, \mathbf{v})$ is given, for all $\mathbf{x} \in \Omega_x$ and $\mathbf{v} \in \Omega_v$. In the forthcoming formulation of the temporal schemes for (8) we omit, for the sake of better readability, the dependence on the variables \mathbf{x} and \mathbf{v} . We consider the following two families of approximate one-step temporal integrators:

1. *Explicit N_{RK} -stage Runge-Kutta methods* (cf. [20] and references therein).

The sequence $\{\mathbf{Y}^\tau(\mathbf{x}, \mathbf{v})\}_\tau$ of numerical solutions of (8) with initial condition \mathbf{Y}^0 is obtained as

$$\begin{aligned} \mathbf{Y}^{\tau+1} &= \varphi_{RK}(\mathbf{Y}^\tau) := \mathbf{Y}^\tau + \Delta t^\tau \sum_{i=1}^{N_{RK}} b_i \mathcal{F}(\mathcal{Y}_i; t^\tau + c_i \Delta t^\tau), \\ \mathcal{Y}_1 &:= \mathbf{Y}^\tau, \\ \mathcal{Y}_i &:= \mathbf{Y}^\tau + \Delta t^\tau \sum_{j=1}^{i-1} a_{ij} \mathcal{F}(\mathcal{Y}_j; t^\tau + c_j \Delta t^\tau), \quad i = 2, \dots, N_{RK}. \end{aligned} \quad (10)$$

The explicit N_{RK} -stage Runge-Kutta method is, thus, characterized by the Runge-Kutta matrix $(a_{ij})_{1 \leq j < i \leq N_{RK}}$ and the set of coefficients $(b_i)_{i=1}^{N_{RK}}, (c_i)_{i=1}^{N_{RK}}$.

2. *Gauss-Legendre methods of order $2N_{GL}$* (cf. [21, Chapter IV.5] and references therein).

Gauss-Legendre temporal integrators are collocation methods based on Gaussian quadrature formulas and belong to the family of implicit Runge-Kutta methods. More specifically, the sequence $\{\mathbf{Y}^\tau(\mathbf{x}, \mathbf{v})\}_\tau$ of numerical solutions of (8) with initial condition \mathbf{Y}^0 is derived as

$$\begin{aligned} \mathbf{Y}^{\tau+1} &= \varphi_{GL}(\mathbf{Y}^\tau) := \mathbf{Y}^\tau + \Delta t^\tau \sum_{i=1}^{N_{GL}} b_i \mathcal{F}(\mathcal{Y}_i; t^\tau + c_i \Delta t^\tau), \\ \mathcal{Y}_i &:= \mathbf{Y}^\tau + \Delta t^\tau \sum_{j=1}^{N_{GL}} a_{ij} \mathcal{F}(\mathcal{Y}_j; t^\tau + c_j \Delta t^\tau), \quad i = 1, \dots, N_{GL}, \end{aligned} \quad (11)$$

with

$$a_{ij} := \int_0^{c_i} \frac{q_j(\sigma)}{q_j(c_j)} d\sigma, \quad b_i := \int_0^1 \frac{q_i(\sigma)}{q_i(c_i)} d\sigma, \quad i, j = 1, \dots, N_{GL},$$

and

$$q_i(\sigma) := \frac{\prod_{j=1}^{N_{GL}} (\sigma - c_j)}{\sigma - c_i}, \quad i = 1, \dots, N_{GL}.$$

The Gauss-Legendre method of order 2 is the implicit midpoint rule. For higher orders, the values of the coefficients $(a_{ij})_{1 \leq i, j \leq N_{GL}}$, $(b_i)_{i=1}^{N_{GL}}$, and $(c_i)_{i=1}^{N_{GL}}$ in (11) can be found in compendia on numerical methods for ordinary differential equations (ODE), see, e.g., [21, Chapter IV.5].

Throughout, we will adopt the shorthand notation $\mathcal{F}_i^N := \mathcal{F}^N(\mathcal{Y}_i; t^\tau + c_i \Delta t^\tau)$.

The choice of an explicit or an implicit temporal integrator is dictated by several factors, and it is usually problem-dependent. Explicit methods are computationally attractive since their implementation to solve (8) only requires N_{RK} evaluations of the function \mathcal{F} per time step: this allows accurate approximations at a competitive computational cost. However, explicit schemes suffer from time step restrictions due to stability requirements and, as problems become increasingly stiff, implicit methods might become more convenient. Moreover, traditional explicit temporal integrators usually fail to preserve at the discrete level the conservation properties of the continuous system. Indeed such schemes are not even guaranteed to preserve polynomial invariants of degree strictly larger than 1. This might trigger spurious behavior of the approximate problem and yield unphysical solutions, particularly for long-time integration.

Implicit temporal integrators exhibit superior stability properties when compared to explicit schemes. In particular, Gauss-Legendre methods are also symmetric and symplectic, and, hence, are well-suited for the approximation of problems over long temporal intervals. Although the stability properties allow for larger time steps, the implementation costs of implicit methods are dominated by the iterative solvers required for the solution of a nonlinear system of equations at each time step. Therefore, the efficiency of implicit methods strongly relies on the availability of fast linear solvers which, for problems featuring a large number of unknowns, also implies the need for efficient preconditioning strategies. The development of efficient solvers is out of the scope of the present work and might provide an interesting direction for future investigation.

4 Hermite-DG approximation of the Vlasov-Maxwell equations in space and velocity

Concerning the discretization in space and velocity of system (8), we consider the spectral-DG method proposed in [29], where Hermite functions provide the spectral approximation of the Vlasov equation in the velocity space, while a discontinuous Galerkin method is used for the spatial discretization. For reader's convenience and to introduce the relevant notation, the method described in [29, Section 3] is briefly summarized in this section. Differently from [29], we present the semi-discretization in space and velocity from an equivalent variational formulation perspective.

The spatial domain Ω_x is partitioned into $N_c = N_x N_y N_z$ cubic or regular hexahedral cells, with N_x , N_y , N_z the number of cells in the x , y , z direction, respectively. We assume that the partition is uniform with mesh size Δx , Δy , and Δz , in each direction, and label the mesh elements by the indices i, j, k running from 1 to N_x , N_y , and N_z , respectively. For convenience of exposition, the generic mesh cell is labeled by the letter I and the summation over all mesh cells is indicated by \sum_I , without the summation bounds being specified. With some abuse of notation, we may subindex I as $I_{i,j,k}$. Accordingly, triplets with an half-integer index, e.g. $(i \pm \frac{1}{2}, j, k)$, $(i, j \pm \frac{1}{2}, k)$ and $(i, j, k \pm \frac{1}{2})$ label the cell interfaces that are orthogonal to the x -, y -, and z -direction, respectively, and delimiting cell $I_{i,j,k}$. With this notation, for example, two consecutive cells in the x -direction are denoted by $I_{i,j,k}$ and $I_{i+1,j,k}$ and are separated by the cell interface $\mathbf{f}_{i+\frac{1}{2},j,k}$. The faces are oriented such that the normal vector to each face always points outwards.

For the spatial discretization, we consider multivariate polynomial functions whose restriction to a given mesh cell I is a polynomial of degree at most N_{DG} . The basis for the local polynomial space $\mathbb{P}_{N_{DG}}(I)$ on the mesh element I are denoted by $\{\varphi^{I,l}\}$ for $l = 1, \dots, N_l$, so that $\mathbb{P}_{N_{DG}}(I) = \text{span}\{\varphi^{I,l}\}_{l=1}^{N_l}$. Here $N_l \in \mathbb{N}_+$ depends on the polynomial degree N_{DG} and on the spatial dimension. We construct the local polynomials $\varphi^{I,l}$ as tensor product of the univariate Legendre polynomials $\{\mathcal{L}_\zeta\}_{\zeta=0}^{N_{DG}}$ of degree ζ , which are defined in the interval $[-1, 1]$ and, then, suitably rescaled and translated on every mesh cell I . The polynomials \mathcal{L}_ζ form an orthogonal basis for $\mathbb{P}_{N_{DG}}([-1, 1])$ [13].

Concerning the spectral approximation in velocity of the Vlasov equation, we consider, as in [29, Section 3.1], the univariate asymmetrically weighted Hermite functions defined as

$$\psi_\zeta(\xi_\beta^s) = (\pi 2^\zeta \zeta!)^{-\frac{1}{2}} \mathcal{H}_\zeta(\xi_\beta^s) \exp(-(\xi_\beta^s)^2), \quad \psi^\zeta(\xi_\beta^s) = (2^\zeta \zeta!)^{-\frac{1}{2}} \mathcal{H}_\zeta(\xi_\beta^s), \quad (12)$$

where $\mathcal{H}_\zeta(\xi_\beta^s)$ is the ζ -th univariate Hermite polynomial in the velocity direction v_β for $\beta(\zeta) \in \{x, y, z\}$, $\zeta \in \{n, m, p\}$ and $n = 0, \dots, N_{v_x}$, $m = 0, \dots, N_{v_y}$, $p = 0, \dots, N_{v_z}$. Moreover, $\boldsymbol{\xi}^s = (\xi_x^s, \xi_y^s, \xi_z^s)^T$, with $\xi_\beta^s = \frac{v_\beta - u_\beta^s}{\alpha_\beta^s}$ with the quantities $u_\beta^s \in \mathbb{R}$ and $\alpha_\beta^s \in \mathbb{R}$ constant factors that depend on the plasma species (and that are specified by the user). The Hermite functions $\Psi_{n,m,p}$ and $\Psi^{n,m,p}$ are given by the tensor product of the univariate Hermite functions (12) as

$$\Psi_{n,m,p}(\boldsymbol{\xi}^s) = \psi_n(\xi_x^s) \psi_m(\xi_y^s) \psi_p(\xi_z^s) \quad \text{and} \quad \Psi^{n,m,p}(\boldsymbol{\xi}^s) = \psi^n(\xi_x^s) \psi^m(\xi_y^s) \psi^p(\xi_z^s).$$

The Hermite-DG variational formulation of the Vlasov-Maxwell system requires the introduction of the following finite dimensional spaces:

$$\begin{aligned} \mathcal{H}^N &:= \text{span}\left\{\Psi_{n,m,p}, \text{ for } (n, m, p) \in \{(0, 0, 0), \dots, (N_{v_x}, N_{v_y}, N_{v_z})\}\right\}, \\ \tilde{\mathcal{H}}^N &:= \text{span}\left\{\Psi^{n,m,p}, \text{ for } (n, m, p) \in \{(0, 0, 0), \dots, (N_{v_x}, N_{v_y}, N_{v_z})\}\right\}, \\ \mathcal{V}^N &:= \text{span}\left\{\varphi^{I,l}, \text{ for } I \equiv I_{i,j,k}, (i, j, k) \in \{(1, 1, 1), \dots, (N_x, N_y, N_z)\}, l = 1, \dots, N_l\right\}. \end{aligned} \quad (13)$$

4.1 Semi-discrete variational formulation

For any time $t \in [0, T]$, we assume that the numerical distribution function $f^{s,N}(\cdot, \cdot, t)$ belongs to $\mathcal{H}^N \times \mathcal{V}^N$ for any plasma species s and therefore it can be written as a linear combination of the Hermite and DG basis functions as

$$f^{s,N}(\mathbf{x}, \mathbf{v}, t) = \sum_{n,m,p} \sum_{I,l} C_{n,m,p}^{s,I,l}(t) \Psi_{n,m,p}(\boldsymbol{\xi}^s) \varphi^{I,l}(\mathbf{x}), \quad \forall t > 0, \mathbf{x} \in \Omega_x, \mathbf{v} \in \Omega_v, \quad (14)$$

where, to ease the notation, we did not specify the summation bounds. Similarly, we take the numerical electromagnetic fields \mathbf{E}^N and \mathbf{B}^N in the finite-dimensional space \mathcal{V}^N . Hence, they admit the expansions

$$\mathbf{E}^N(\mathbf{x}, t) = \sum_{I,l} \mathbf{E}^{I,l}(t) \varphi^{I,l}(\mathbf{x}), \quad \forall t > 0, \mathbf{x} \in \Omega_x, \quad (15)$$

$$\mathbf{B}^N(\mathbf{x}, t) = \sum_{I,l} \mathbf{B}^{I,l}(t) \varphi^{I,l}(\mathbf{x}), \quad \forall t > 0, \mathbf{x} \in \Omega_x, \quad (16)$$

where $\mathbf{E}^{I,l}(t) = (E_x^{I,l}(t), E_y^{I,l}(t), E_z^{I,l}(t))^T$ and $\mathbf{B}^{I,l}(t) = (B_x^{I,l}(t), B_y^{I,l}(t), B_z^{I,l}(t))^T$ are the DG expansion coefficients of the spatial components of the electric and magnetic fields, $\mathbf{E}^N = (E_x^N, E_y^N, E_z^N)^T$ and $\mathbf{B}^N = (B_x^N, B_y^N, B_z^N)$, respectively.

The semi-discrete variational formulation of the Hermite-DG method reads as: *For every species s , and any time $t \in (0, T]$, find $f^{s,N}(\cdot, \cdot, t) \in \mathcal{H}^N \times \mathcal{V}^N$ and $\mathbf{E}^N(\cdot, t), \mathbf{B}^N(\cdot, t) \in \mathcal{V}^N$ such that*

$$\mathcal{A}((f^{s,N}, \mathbf{E}^N, \mathbf{B}^N), (\Psi, \varphi)) = 0 \quad \forall (\Psi, \varphi) \in \tilde{\mathcal{H}}^N \times \mathcal{V}^N, \quad (17a)$$

$$\mathcal{B}((\mathbf{E}^N, \mathbf{B}^N), \varphi) = \mathcal{L}(\varphi) \quad \forall \varphi \in \mathcal{V}^N, \quad (17b)$$

$$f^{s,N}(\cdot, \cdot, 0) = f_0^{s,N} \quad \text{in } \Omega_x \times \Omega_v, \quad (17c)$$

$$\mathbf{E}^N(\cdot, 0) = \mathbf{E}_0^N \quad \text{in } \Omega_x, \quad (17d)$$

$$\mathbf{B}^N(\cdot, 0) = \mathbf{B}_0^N \quad \text{in } \Omega_x, \quad (17e)$$

where $f_0^{s,N}$, \mathbf{E}_0^N and \mathbf{B}_0^N are the orthogonal projections of the initial conditions $f^s(\cdot, \cdot, 0)$, $\mathbf{E}(\cdot, 0)$ and $\mathbf{B}(\cdot, 0)$ onto the spaces $\mathcal{H}^N \times \mathcal{V}^N$, \mathcal{V}^N and \mathcal{V}^N , respectively, and suitable boundary conditions are prescribed on $\partial\Omega_x$.

To define the multilinear form \mathcal{A} in (17a), we first introduce the auxiliary vector function

$$\mathbf{g}_\Psi^{s,N}(\mathbf{x}, t) := \int_{\Omega_v} \mathbf{v} f^{s,N}(\mathbf{x}, \mathbf{v}, t) \Psi(\boldsymbol{\xi}) d\boldsymbol{\xi}, \quad \forall \Psi \in \tilde{\mathcal{H}}^N.$$

Then, for any $f^{s,N} \in \mathcal{H}^N \times \mathcal{V}^N$, $\mathbf{E}^N \in \mathcal{V}^N$, $\mathbf{B}^N \in \mathcal{V}^N$, and $(\Psi, \varphi) \in \tilde{\mathcal{H}}^N \times \mathcal{V}^N$, we define

$$\begin{aligned} \mathcal{A}((f^{s,N}, \mathbf{E}^N, \mathbf{B}^N), (\Psi, \varphi)) &:= \sum_I \left(\int_I \int_{\Omega_v} \frac{\partial f^{s,N}}{\partial t} \Psi(\boldsymbol{\xi}) \varphi(\mathbf{x}) d\boldsymbol{\xi} d\mathbf{x} - \int_I \mathbf{g}_\Psi^{s,N} \cdot \nabla_{\mathbf{x}} \varphi(\mathbf{x}) d\mathbf{x} \right. \\ &\quad \left. + \int_{\partial I} \widehat{\mathbf{n} \cdot \mathbf{g}_\Psi^{s,N}} \varphi(\mathbf{x}) dS + \frac{q^s \omega_{ce}}{m^s \omega_{pe}} \int_I \int_{\Omega_v} (\mathbf{E}^N + \mathbf{v} \times \mathbf{B}^N) \cdot \nabla_{\mathbf{v}} f^{s,N} \Psi(\boldsymbol{\xi}) \varphi(\mathbf{x}) d\boldsymbol{\xi} d\mathbf{x} \right). \end{aligned} \quad (18)$$

Concerning the discretization of Maxwell's equations in (17b), we first consider the fluxes of the conservative formulation (6), and observe that, if we partition the vector flux $\mathbb{F}(\mathbf{u})$ in a column-wise form, so that

$$\nabla_{\mathbf{x}} \cdot \mathbb{F}(\mathbf{u}) = \frac{\partial}{\partial x} \mathbf{F}_x(\mathbf{u}) + \frac{\partial}{\partial y} \mathbf{F}_y(\mathbf{u}) + \frac{\partial}{\partial z} \mathbf{F}_z(\mathbf{u}), \quad (19)$$

we can write $\mathbf{F}_x(\mathbf{u}) = \mathbb{F}_x \mathbf{u}$, $\mathbf{F}_y(\mathbf{u}) = \mathbb{F}_y \mathbf{u}$, and $\mathbf{F}_z(\mathbf{u}) = \mathbb{F}_z \mathbf{u}$, with flux matrices $\mathbb{F}_x, \mathbb{F}_y, \mathbb{F}_z \in \mathbb{R}^{6 \times 6}$ defined as in [29, Eqs. (50)-(52)]. Let $\mathbf{n} = (n_x, n_y, n_z)^T$ be a generic vector in \mathbb{R}^3 . We use the notation $\mathbb{F}(\mathbf{u})\mathbf{n}$ to indicate $\mathbb{F}(\mathbf{u})\mathbf{n} := \mathbf{F}_x(\mathbf{u})n_x + \mathbf{F}_y(\mathbf{u})n_y + \mathbf{F}_z(\mathbf{u})n_z$, and use an analogous definition for $\mathbb{F}_{\mathbf{E}}(\mathbf{u})\mathbf{n}$ and $\mathbb{F}_{\mathbf{B}}(\mathbf{u})\mathbf{n}$. Using [29, Eq. (53)], one has $\mathbb{F}_{\mathbf{E}}(\mathbf{u})\mathbf{n} \cdot \mathbf{E} = \mathbb{F}_{\mathbf{B}}(\mathbf{u})\mathbf{n} \cdot \mathbf{B} = \mathbf{n} \cdot (\mathbf{E} \times \mathbf{B})$.

Let $\mathbf{U}(t) := ((\mathbf{E}^N)^T, (\mathbf{B}^N)^T)^T$ denote the DG approximation of the vector-valued function \mathbf{u} in (4). The bilinear form associated with the discretization of Maxwell's equations is

$$\mathcal{B}((\mathbf{E}^N, \mathbf{B}^N), \varphi) := \mathcal{B}_{\mathbf{E}}((\mathbf{E}^N, \mathbf{B}^N), \varphi) + \mathcal{B}_{\mathbf{B}}((\mathbf{E}^N, \mathbf{B}^N), \varphi), \quad \forall \mathbf{E}^N, \mathbf{B}^N, \varphi \in \mathcal{V}^N, \quad (20)$$

where

$$\mathcal{B}_{\mathbf{E}}((\mathbf{E}^N, \mathbf{B}^N), \varphi) = \sum_I \left(\int_I \frac{\partial \mathbf{E}^N}{\partial t} \varphi(\mathbf{x}) d\mathbf{x} - \int_I \mathbb{F}_{\mathbf{E}}(\mathbf{U}) \nabla_{\mathbf{x}} \varphi(\mathbf{x}) d\mathbf{x} + \int_{\partial I} \widehat{\mathbb{F}_{\mathbf{E}}(\mathbf{U})\mathbf{n}} \varphi(\mathbf{x}) dS \right), \quad (21)$$

$$\mathcal{B}_{\mathbf{B}}((\mathbf{E}^N, \mathbf{B}^N), \varphi) = \sum_I \left(\int_I \frac{\partial \mathbf{B}^N}{\partial t} \varphi(\mathbf{x}) d\mathbf{x} - \int_I \mathbb{F}_{\mathbf{B}}(\mathbf{U}) \nabla_{\mathbf{x}} \varphi(\mathbf{x}) d\mathbf{x} + \int_{\partial I} \widehat{\mathbb{F}_{\mathbf{B}}(\mathbf{U})\mathbf{n}} \varphi(\mathbf{x}) dS \right). \quad (22)$$

The linear functional \mathcal{L} in (17b) is defined, for all $\varphi \in \mathcal{V}^N$, as

$$\mathcal{L}(\varphi) := -\frac{\omega_{pe}}{\omega_{ce}} \sum_I \int_I \mathbf{J}^N(\mathbf{x}, t) \varphi(\mathbf{x}) d\mathbf{x}, \quad \mathbf{J}^N(\mathbf{x}, t) = \sum_s q^s \int_{\Omega_v} \mathbf{v} f^{s,N}(\mathbf{x}, \mathbf{v}, t) d\mathbf{v}.$$

The quantity $\widehat{\mathbf{n} \cdot \mathbf{g}_{\Psi}^{s,N}}$ in (18) and $\widehat{\mathbb{F}_{\mathbf{E}}(\mathbf{U})\mathbf{n}}$ and $\widehat{\mathbb{F}_{\mathbf{B}}(\mathbf{U})\mathbf{n}}$ in (21)-(22) are the numerical fluxes at the interfaces of the element boundaries. At the boundaries of the domain Ω_x these quantities are defined in accordance with the prescribed boundary conditions. We consider two different kinds of numerical fluxes for Maxwell's equations, the *central numerical flux* and the *upwind numerical flux*, while the Vlasov equation is treated with the upwind numerical flux. We remark that the choice of the numerical flux plays a crucial role in the conservation properties of the resulting semi-discrete problem and, hence, in the construction of the numerical time integrators, as it will be shown in Section 6. We provide a brief description of the numerical treatment of the boundary integral in the x direction, and, in particular, at the face $\mathbf{f}_{i+\frac{1}{2},j,k}$. We refer to [29, Section 4] for a detailed derivation. Figure 1 illustrates the meaning of the main symbols that we adopt in the paper. Let $\mathbf{n} = (n_x, n_y, n_z)^T$ be the unit vector that is orthogonal to the boundary ∂I of I and $\mathbf{n}_{\mathbf{f}_*}$ the normal vector to the face \mathbf{f}_* indicated by a specific triple of indices, e.g., $\mathbf{n}_{\mathbf{f}_{i+\frac{1}{2},j,k}}$. Since, by construction, $n_x = \pm 1$, $n_y = n_z = 0$ on the two faces $\mathbf{f}_{i\pm\frac{1}{2},j,k}$, we obtain,

$$\int_{\partial_x I} n_x \mathbf{F}_x(\mathbf{U}) \varphi^{I,l}(\mathbf{x}) dS = \int_{\mathbf{f}_{i+\frac{1}{2},j,k}} \mathbf{F}_x(\mathbf{U}) \varphi^{I,l}(x_{i+\frac{1}{2}}, y, z) dy dz - \int_{\mathbf{f}_{i-\frac{1}{2},j,k}} \mathbf{F}_x(\mathbf{U}) \varphi^{I,l}(x_{i-\frac{1}{2}}, y, z) dy dz.$$

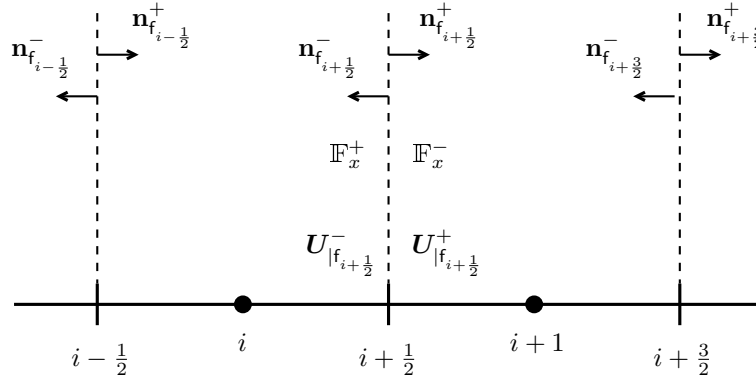


Figure 1: Notation of the numerical flux functions along direction x . The normal vectors $\mathbf{n}_{\mathbf{f}_\ell}^+$ are oriented along the positive real axis (from left to right); vectors $\mathbf{n}_{\mathbf{f}_\ell}^-$ are in the opposite sense. At the interface $\mathbf{f}_{i+\frac{1}{2}}$, the matrix $\mathbb{F}_x = \mathbb{F}_x^+ + \mathbb{F}_x^-$ is decomposed into characteristics waves traveling from left to right, \mathbb{F}_x^+ , which transport solution \mathbf{U}^- from inside cell i toward the cell interface, and from right to left, \mathbb{F}_x^- , which transport the solution \mathbf{U}^+ from inside cell $i + 1$ towards the cell interface. Here $\mathbf{U}_{|f_{i+\frac{1}{2}}}^\pm$ are shortcut notations for $\mathbf{U}(x_{i+\frac{1}{2}}^\pm, y, z, t)$.¹

Let $\mathbf{U}(\mathbf{x}_{i+\frac{1}{2},j,k}^\pm, t)$ denote $\lim_{\epsilon \rightarrow 0} \mathbf{U}(\mathbf{x}_{i+\frac{1}{2},j,k} \pm \epsilon \mathbf{n}_{\mathbf{f}_{i+\frac{1}{2},j,k}}, t)$. Then,

- the *central numerical flux* is given by the formula:

$$\widehat{\mathbb{F}_x \mathbf{U}}(\mathbf{x}_{i+\frac{1}{2},j,k}, t) = \mathbb{F}_x \frac{1}{2} (\mathbf{U}(\mathbf{x}_{i+\frac{1}{2},j,k}^-, t) + \mathbf{U}(\mathbf{x}_{i+\frac{1}{2},j,k}^+, t)); \quad (23)$$

- the *upwind numerical flux* is based on the characteristic decomposition of the flux matrices: $\mathbb{F}_\beta = \mathbb{F}_\beta^+ + \mathbb{F}_\beta^-$, for each $\beta \in \{x, y, z\}$. We perform such decomposition numerically as described in [29, Remark 3.4]. On face $\mathbf{f}_{i+\frac{1}{2},j,k}$, we approximate the flux integral using the upwind flux decomposition of the matrix \mathbb{F}_x as follows

$$\widehat{\mathbb{F}_x \mathbf{U}}(\mathbf{x}_{i+\frac{1}{2},j,k}, t) = \underbrace{\mathbb{F}_x^+ \mathbf{U}(\mathbf{x}_{i+\frac{1}{2}}^-, y, z, t)}_{\text{from cell } I = I_{i,j,k}} + \underbrace{\mathbb{F}_x^- \mathbf{U}(\mathbf{x}_{i+\frac{1}{2}}^+, y, z, t)}_{\text{from cell } I^+ = I_{i+1,j,k}}. \quad (24)$$

Remark 4.1 (Consistency). Since upwind and central numerical fluxes are consistent whenever the associated physical flux is sufficiently regular, the Hermite-DG discretization (17) is consistent. This

¹Figure reprinted from [29], with permission from Elsevier.

means that, if the exact solution fields f^s , \mathbf{E} , \mathbf{B} , and \mathbf{J} are sufficiently regular (at least continuous), then they satisfy the variational problem

$$\begin{aligned}\mathcal{A}((f^s, \mathbf{E}, \mathbf{B}), (\Psi, \varphi)) &= 0 \quad \forall (\Psi, \varphi) \in \tilde{\mathcal{H}}^N \times \mathcal{V}^N, \\ \mathcal{B}((\mathbf{E}, \mathbf{B}), \varphi) &= \mathcal{L}(\varphi) \quad \forall \varphi \in \mathcal{V}^N,\end{aligned}$$

defined in the finite dimensional spaces \mathcal{H}^N , $\tilde{\mathcal{H}}^N$, and \mathcal{V}^N .

5 Semi-discrete problem and conservation properties of the Hermite-DG scheme

With the Hermite-DG discretization (17a)-(17b) of the Vlasov-Maxwell equations, we can derive the semi-discrete formulation of the evolution problem (8). Analogously to (7), we introduce the finite-dimensional vector of unknowns defined, for any $t \in [0, T]$, as

$$y(t) = \begin{pmatrix} (C_{n,m,p}^{s,I,l}(t))_{n,m,p}^{s,I,l} \\ (\mathbf{E}^{I,l}(t))_{I,l} \\ (\mathbf{B}^{I,l}(t))_{I,l} \end{pmatrix} \in \mathbb{R}^M, \quad (25)$$

where the coefficients $C_{n,m,p}^{s,I,l}(t)$ are defined in (14), the coefficients $\mathbf{E}^{I,l}(t)$ in (15), and the coefficients $\mathbf{B}^{I,l}(t)$ in (16). Testing equations (17a)-(17b) against the basis functions $\{\Psi^{n,m,p}\}$ in $\tilde{\mathcal{H}}^N$ and $\{\phi^{I,l}\}$ in \mathcal{V}^N yields an autonomous system of ordinary differential equations that can formally be written as

$$y'(t) = \mathcal{F}^N(y(t); t) \quad \text{in } (0, T], \quad (26)$$

where \mathcal{F}^N corresponds to the Hermite-DG discretization of (9), and a suitable initial condition $y(0)$ is provided. We assume that, for a fixed initial condition $y(0)$, the solution $y(t)$ at time $t \in (0, T]$ exists and is unique.

The fully discrete approximation of the Vlasov-Maxwell equations is then obtained by solving (26) with one of the RK methods introduced in Section 3, after setting $y^0 = y(0)$.

5.1 Invariants and conservation properties

In order to study the conservation properties of the fully discrete problem, we consider polynomial conserved quantities of a dynamical system. Suppose that $\mathcal{I} \in C^\infty(\mathbb{R}^M)$ is an invariant of the autonomous ODE (26). Then, \mathcal{I} is called a *polynomial invariant* of degree p if it is a polynomial of degree at most p in the variable $y \in \mathbb{R}^M$, namely $\mathcal{I} \in \mathbb{P}_p(\mathbb{R}^M)$. For $p = 1$ we call \mathcal{I} a linear invariant and it is of the form $\mathcal{I}(y) = \mu^\top y + c$, where $\mu \in \mathbb{R}^M$ and $c \in \mathbb{R}$. For $p = 2$, we have a quadratic invariant that can be written as $\mathcal{I}(y) = y^\top S y + \mu^\top y + c$, for $S \in \mathbb{R}^{M \times M}$ symmetric, $\mu \in \mathbb{R}^M$ and $c \in \mathbb{R}$.

The conservation laws of general physical systems might not be expressed as invariants of motion in the classical sense, since they might need to take into account the exchanges of the system with the external ambient space. The flux of a quantity at the boundary of the domain contributes to a conservation law as an integral over the temporal interval that expresses the balance between what has entered and what has left the domain during the system evolution. In this case, we talk about conservation laws *in weak form*, as specified in the following definition.

Definition 5.1. Let $\mathcal{D}, \mathcal{C} : \mathbb{R}^M \rightarrow \mathbb{R}$ be given functions of $y : [0, T] \rightarrow \mathbb{R}^M$. A quantity of the form

$$\mathcal{I}(y(t), t) := \mathcal{D}(y(t)) + \int_0^t \mathcal{C}(y(s)) ds, \quad (27)$$

provides a conservation law in weak form if it satisfies

$$\frac{d\mathcal{I}(y(t), t)}{dt} = 0, \quad \forall y(t) \in \mathbb{R}^M. \quad (28)$$

Notice that if \mathcal{C} in (27) is identically zero, then $\mathcal{I}(y(t), t) = \mathcal{D}(y(t))$ is an invariant of motion of (26) in the classical sense.

The Vlasov-Maxwell equations possess an infinite set of conserved quantities in weak form, among those, the number of particles, the total momentum, and the total energy. In the notation of Definition 5.1, these quantities are encoded in the function \mathcal{D} . The term \mathcal{C} , instead, describes the flux of the conserved quantity at the boundaries of the computational domain and it is associated with the possible presence of sources. The term \mathcal{C} also takes into account the numerical contributions to the conserved quantity \mathcal{D} that result from the numerical approximation of the Vlasov-Maxwell equations in space and velocity.

In the next subsections, we study the conservation laws associated with the total number of particles and the total energy for the Vlasov-Maxwell system (1), (2) and (3). Note that we do not consider the conservation of total momentum since this quantity is already not conserved at the level of the semi-discrete system, as demonstrated in Ref. [29]. For each of these, we characterize the corresponding conserved quantity of the ODE (26), obtained from the approximation of the continuous conservation laws. Finally, in Section 6, we analyze the capability of each RK temporal integrator introduced in Section 3 to preserve such quantities.

The conservation properties of the semi-discrete scheme (17) were already studied in [29]. Here we characterize them as conservation properties of (26), in the sense of Definition 5.1, and we refer the reader to [29] for further details. To fix the notation, for the generic quantity $\Phi^N(\mathbf{x}, \mathbf{v}, t)$ involved in the discretization of the Vlasov-Maxwell equations (17a)-(17b), we use the superscript τ to indicate its approximation at time t^τ , namely $\Phi^{N,\tau}(\mathbf{x}, \mathbf{v}) \approx \Phi^N(\mathbf{x}, \mathbf{v}, t^\tau)$.

5.2 Number of particles

Lemma 5.1. *Let $f^{s,N}(\mathbf{x}, \mathbf{v}, t)$ be the numerical solution of the semi-discrete Vlasov-Maxwell problem (17) and let $y(t)$ be as in (25) for $t \in [0, T]$. The approximate number of particles of each plasma species s ,*

$$\mathcal{N}^s(y(t)) = \sum_I \int_I \int_{\Omega_v} f^{s,N}(\mathbf{x}, \mathbf{v}, t) d\mathbf{x} d\mathbf{v}, \quad (29)$$

satisfies

$$\frac{d\mathcal{N}^s(y(t))}{dt} + \int_{\partial\Omega_x} \int_{\Omega_v} (\mathbf{n} \cdot \mathbf{v}) f^{s,N}(\mathbf{x}, \mathbf{v}, t) d\mathbf{v} dS = 0, \quad \forall s. \quad (30)$$

An analogous result holds for the total number of particles in the plasma $\mathcal{N}^{tot} := \sum_s \mathcal{N}^s$. Notice that the integral term in (30) is the flux of particles at the boundary of Ω_x and represents the balance between the number of particles entering the domain and the particles leaving the domain at time t . This quantity vanishes when periodic boundary conditions are imposed or when the plasma is entirely confined to Ω_x .

The approximate number of particles \mathcal{N}^s of a given plasma species s is a linear function of the vector y whose components are specified in (25). Indeed, the Hermite-DG expansion (14) of $f^{s,N}$ yields

$$\mathcal{N}^s(y) = \sum_I \int_I \int_{\Omega_v} f^{s,N}(\mathbf{x}, \mathbf{v}, t) d\mathbf{x} d\mathbf{v} = \Delta x \Delta y \Delta z \alpha_x^s \alpha_y^s \alpha_z^s \sum_I C_{0,0,0}^{s,I,0}.$$

5.3 Total energy

In the continuum, the total energy of the Vlasov-Maxwell problem is defined as

$$\mathcal{E} := \frac{1}{2} \sum_s m^s \int_{\Omega_x} \int_{\Omega_v} |\mathbf{v}|^2 f^s(\mathbf{x}, \mathbf{v}, t) d\mathbf{v} d\mathbf{x} + \frac{1}{2} \left(\frac{\omega_{ce}}{\omega_{pe}} \right)^2 \int_{\Omega_x} (|\mathbf{E}(\mathbf{x}, t)|^2 + |\mathbf{B}(\mathbf{x}, t)|^2) d\mathbf{x}.$$

To derive a conservation law for (26) associated with the total energy we consider, for y defined as in (25), the following quantities,

$$\mathcal{E}_{\text{kin}}(y) := \frac{1}{2} \sum_s m^s \sum_I \int_I \int_{\Omega_v} |\mathbf{v}|^2 f^{s,N}(\mathbf{x}, \mathbf{v}, t) d\mathbf{v} d\mathbf{x}, \quad (31)$$

$$\mathcal{E}_{\mathbf{E}, \mathbf{B}}(y) := \frac{1}{2} \left(\frac{\omega_{ce}}{\omega_{pe}} \right)^2 \sum_I \int_I \left(|\mathbf{E}^N(\mathbf{x}, t)|^2 + |\mathbf{B}^N(\mathbf{x}, t)|^2 \right) d\mathbf{x}, \quad (32)$$

$$\mathcal{E}_{\text{jump}}(y) := \left(\frac{\omega_{ce}}{\omega_{pe}} \right)^2 \sum_{\mathbf{f}} \mathcal{J}_{\mathbf{f}}(y(t)), \quad (33)$$

$$\mathcal{E}_{\text{bnd}}(y) := \frac{1}{2} \sum_s m^s \int_{\partial\Omega_x} \int_{\Omega_v} (\mathbf{n} \cdot \mathbf{v}) |\mathbf{v}|^2 f^{s,N}(\mathbf{x}, \mathbf{v}, t) d\mathbf{v} dS. \quad (34)$$

The first two quantities \mathcal{E}_{kin} and $\mathcal{E}_{\mathbf{E}, \mathbf{B}}$ are the approximate kinetic and electromagnetic energy. The remaining quantities (33) and (34) are associated with the energy flux at the domain boundaries and mesh interfaces. Specifically, term (34) describes the exchange of kinetic energy at the boundaries of the domain Ω_x at time t , while term $\mathcal{J}_{\mathbf{f}}$ in (33) is defined as

$$\mathcal{J}_{\mathbf{f}}(y(t)) := \begin{cases} 0 & \text{for the central numerical flux (23),} \\ \frac{1}{2} \int_{\mathbf{f}} \llbracket \mathbf{U}(t) \rrbracket_{\mathbf{f}}^\top \cdot |\mathbb{F}| \cdot \llbracket \mathbf{U}(t) \rrbracket_{\mathbf{f}} dS & \text{for the upwind numerical flux (24),} \end{cases} \quad (35)$$

where $|\mathbb{F}| = |\mathbb{F}_x| + |\mathbb{F}_y| + |\mathbb{F}_z|$ with $|\mathbb{F}_\beta| = \mathbb{F}_\beta^+ - \mathbb{F}_\beta^-$, for $\beta \in \{x, y, z\}$, and

$$\llbracket \mathbf{U}(t) \rrbracket_{\mathbf{f}} = \mathbf{n}^+ \cdot \mathbf{U}(\mathbf{x}_{\mathbf{f}}^+, t) + \mathbf{n}^- \cdot \mathbf{U}(\mathbf{x}_{\mathbf{f}}^-, t) =: \mathbf{n}^+ \cdot \mathbf{U}_{\mathbf{f}}^+(t) + \mathbf{n}^- \cdot \mathbf{U}_{\mathbf{f}}^-(t),$$

is the jump of \mathbf{U} across the mesh face \mathbf{f} , and $\mathbf{U}_{\mathbf{f}}^\pm(t) = \mathbf{U}(\mathbf{x}_{\mathbf{f}}^\pm, t)$ denotes the trace of \mathbf{U} on opposite sides of \mathbf{f} . Note that Eq. (33) depends only on the jumps at the mesh interfaces of the electromagnetic field. The fluxes at the mesh interfaces associated with the Vlasov equation do not enter the time derivative of the kinetic energy (since it is a linear quantity and one can take advantage of properties of telescopic sums). Hence, the fact that we use upwind fluxes for the Vlasov equation does not affect explicitly the conservation of energy. Note, also, that the energy flux (34) at the domain boundaries vanishes whenever periodic boundary conditions are prescribed.

The following result was shown in [29, Theorem 5.3] under the assumption of periodic boundary conditions on $\partial\Omega_x$, and we report it here, without proof, in the more general setting with arbitrary boundary conditions.

Lemma 5.2. *Let $y(t)$ be the numerical solution at time $t \in (0, T]$ of the semi-discrete Vlasov-Maxwell problem (26) with initial condition $y(0)$. Let \mathcal{E}_{kin} and $\mathcal{E}_{\mathbf{E}, \mathbf{B}}$ be the discrete kinetic and electromagnetic energies introduced in (31) and (32), respectively. The variation in time of the total discrete energy of the system defined as*

$$\mathcal{E}_{\text{tot}}(y) = \mathcal{E}_{\text{kin}}(y) + \mathcal{E}_{\mathbf{E}, \mathbf{B}}(y), \quad (36)$$

satisfies

$$\frac{d\mathcal{E}_{\text{tot}}(y(t))}{dt} + \frac{1}{2} \sum_s m^s \int_{\partial\Omega_x} \int_{\Omega_v} (\mathbf{n} \cdot \mathbf{v}) |\mathbf{v}|^2 f^{s,N}(\mathbf{x}, \mathbf{v}, t) d\mathbf{v} dS = - \left(\frac{\omega_{ce}}{\omega_{pe}} \right)^2 \sum_{\mathbf{f}} \mathcal{J}_{\mathbf{f}}(y(t)) \leq 0, \quad (37)$$

where $\mathcal{J}_{\mathbf{f}}$ is defined in (35).

In other words, the quantity

$$\mathcal{E}_{\text{mod}}(y(t)) := \mathcal{E}_{\text{kin}}(y(t)) + \mathcal{E}_{\mathbf{E}, \mathbf{B}}(y(t)) + \int_0^t \mathcal{E}_{\text{bnd}}(y(\sigma)) d\sigma + \int_0^t \mathcal{E}_{\text{jump}}(y(\sigma)) d\sigma, \quad (38)$$

is conserved in the sense of (27), (28) for the evolution problem (26). When central numerical fluxes are used in Maxwell's equations, the last term vanishes and \mathcal{E}_{mod} coincides with the semi-discrete total energy which is then conserved. Instead, the term $\mathcal{E}_{\text{jump}}$, appearing when upwind numerical fluxes are used in Maxwell's equations, corresponds to a numerical dissipation and hence, in this case, the semi-discrete total energy is not conserved.

The total energy (36) is a quadratic function of the vector unknown y whose components are specified in (25). Indeed, the kinetic energy can be expressed in the components of y as

$$\begin{aligned} \mathcal{E}_{\text{kin}}(y) = \frac{1}{4} \Delta x \Delta y \Delta z \sum_s \alpha_x^s \alpha_y^s \alpha_z^s m^s \sum_I \left[\sum_{\beta \in \{x,y,z\}} ((\alpha_\beta^s)^2 + 2(u_\beta^s)^2) C_{0,0,0}^{s,I,0} + 2\sqrt{2} \alpha_x^s u_x^s C_{1,0,0}^{s,I,0} \right. \\ \left. + (\alpha_x^s)^2 C_{2,0,0}^{s,I,0} + 2\sqrt{2} \alpha_y^s u_y^s C_{0,1,0}^{s,I,0} + (\alpha_y^s)^2 C_{0,2,0}^{s,I,0} + 2\sqrt{2} \alpha_z^s u_z^s C_{0,0,1}^{s,I,0} + (\alpha_z^s)^2 C_{0,0,2}^{s,I,0} \right]. \end{aligned}$$

The kinetic energy is linear in y so that $\mathcal{E}_{\text{kin}}(y) = \mu^\top y$ where $\mu \in \mathbb{R}^M$ can be derived from the expression above by using a suitable application that maps the indices (s, I, l, n, m, p) into a single integer index in $[1, M]$. Concerning the electromagnetic energy, the orthogonality properties of the Legendre polynomials yield

$$\mathcal{E}_{E,B}(y) = \frac{1}{2} \left(\frac{\omega_{ce}}{\omega_{pe}} \right)^2 \Delta x \Delta y \Delta z \sum_{I,l} [(E^{I,l})^2 + (B^{I,l})^2].$$

Hence, $\mathcal{E}_{E,B}(y) = y^\top S y$ where $S \in \mathbb{R}^{M \times M}$ is the zero matrix in the part that multiplies the components $(C_{n,m,p}^{s,I,l})$ of y and it is the identity matrix in the part that multiplies the DG degrees of freedom of the electromagnetic fields.

6 Conservation properties of the fully discrete Vlasov-Maxwell equations

This section pertains to the conservation of invariants and balance laws in weak form by the numerical time integrators introduced in Section 3, when applied to the semi-discrete problem (26) ensuing from the Hermite-DG discretization (17) of the Vlasov-Maxwell equations.

Definition 6.1. A numerical time integrator preserves polynomial invariants of degree p if, for any autonomous ODE of the form (26) with an invariant $\mathcal{I} \in \mathbb{P}_p(\mathbb{R}^M)$, the function \mathcal{I} satisfies

$$\mathcal{I}(y^\tau) = \mathcal{I}(y^0), \quad \forall \tau,$$

where y^τ is the approximate solution of (26) at time t^τ with initial condition $y^0 \in \mathbb{R}^M$.

A complete characterization of Runge-Kutta methods that preserve polynomial invariants can be found in [19, Chapter IV]. In particular, all explicit and implicit RK methods preserve linear invariants, and all GL methods preserve quadratic invariants, [7].

In the following result, we characterize the conservation properties of Runge-Kutta methods when dealing with conservation laws in weak form, in the sense of Definition 5.1.

Theorem 6.1. Let $\mathcal{D}, \mathcal{C} : \mathbb{R}^M \rightarrow \mathbb{R}$ be given functions of $y : [0, T] \rightarrow \mathbb{R}^M$. Assume that the quantity

$$\mathcal{I}(y(t), t) := \mathcal{D}(y(t)) + \int_0^t \mathcal{C}(y(s)) ds,$$

satisfies a conservation law in weak form in the sense of Definition 5.1, namely

$$\frac{d\mathcal{I}(y(t), t)}{dt} = \frac{d\mathcal{D}(y(t))}{dt} + \mathcal{C}(y(t)) = 0, \quad (39)$$

for every $y(t) \in \mathbb{R}^M$. Consider the two cases:

1. $\{y^\tau\}_{\tau=1,\dots,T/\Delta t}$ is the sequence of numerical solutions of (26) with initial condition y^0 , obtained with an explicit RK scheme of the family (10). Assume, then, that \mathcal{I} is linear in y and let $N_T = N_{RK}$.
2. $\{y^\tau\}_{\tau=1,\dots,T/\Delta t}$ is the sequence of numerical solutions of (26) with initial condition y^0 , obtained with a GL scheme of the family (11). Assume, in this case, that \mathcal{I} is at most quadratic in y and let $N_T = N_{GL}$.

Under the assumptions above, it holds that

$$\mathcal{D}(y^{\tau+1}) = \mathcal{D}(y^\tau) - \Delta t \sum_{i=1}^{N_T} b_i \mathcal{C}(\mathcal{Y}_i), \quad \forall \tau, \quad (40)$$

where $(\mathcal{Y}_i)_{i=1}^{N_T}$ are defined in (10) for case (i) and in (11) for case (ii). Equation (40) is the discrete equivalent of Eq. (39) and expresses the conservation law in weak form for the family of RK methods.

Proof. Since the quantity \mathcal{I} , and hence \mathcal{D} , is assumed to be at most quadratic in y we can recast it as $\mathcal{D}(y) = y^\top S y + \mu^\top y + \eta$, for $\mu \in \mathbb{R}^M$, $\eta \in \mathbb{R}$ and a symmetric matrix $S \in \mathbb{R}^{M \times M}$ that is identically zero when \mathcal{I} is linear, as assumed in case (i). Using the definition of temporal integrator in (10) and (11), we have $y^{\tau+1} = y^\tau + \delta y^\tau$ with

$$\delta y^\tau := \Delta t \sum_{i=1}^{N_T} b_i \mathcal{F}_i^N, \quad (41)$$

with $\mathcal{F}_i^N := \mathcal{F}^N(\mathcal{Y}_i; t^\tau + c_i \Delta t^\tau)$, and N_T either equal to N_{RK} or N_{GL} . Then,

$$\mathcal{D}(y^{\tau+1}) = (y^{\tau+1})^\top S y^{\tau+1} + \mu^\top y^{\tau+1} + \eta = \mathcal{D}(y^\tau) + 2(y^\tau)^\top S \delta y^\tau + (\delta y^\tau)^\top S \delta y^\tau + \mu^\top \delta y^\tau,$$

where, due to the symmetry of S , we have used $(y^\tau)^\top S \delta y^\tau = (\delta y^\tau)^\top S y^\tau$. The definition of δy^τ yields

$$\mathcal{D}(y^{\tau+1}) = \mathcal{D}(y^\tau) + 2\Delta t \sum_{i=1}^{N_T} b_i (y^\tau)^\top S \mathcal{F}_i^N + \Delta t^2 \sum_{i,j=1}^{N_T} b_i b_j (\mathcal{F}_i^N)^\top S \mathcal{F}_j^N + \Delta t \sum_{i=1}^{N_T} b_i \mu^\top \mathcal{F}_i^N. \quad (42)$$

Using the formula $\mathcal{Y}_i = y^\tau + \Delta t \sum_{j=1}^{N_T} a_{ij} \mathcal{F}_j^N$ to substitute y^τ in (42), results in

$$\mathcal{D}(y^{\tau+1}) = \mathcal{D}(y^\tau) + \Delta t \sum_{i=1}^{N_T} b_i (\mu^\top + 2\mathcal{Y}_i^\top S) \mathcal{F}_i^N + \Delta t^2 \sum_{i,j=1}^{N_T} (b_i b_j - a_{ij} b_i - a_{ji} b_j) (\mathcal{F}_i^N)^\top S \mathcal{F}_j^N. \quad (43)$$

Here, when $N_T = N_{RK}$, $a_{ij} = 0$ for any $j \geq i$. Assumption (39), together with (26), yield

$$-\mathcal{C}(y(t)) = \frac{d\mathcal{D}(y(t))}{dt} = \frac{d}{dt} (y^\top S y + \mu^\top y) = (\mu^\top + 2y^\top S) \frac{dy}{dt} = (\mu^\top + 2y^\top S) \mathcal{F}^N(y), \quad \forall y. \quad (44)$$

Taking $y = \mathcal{Y}_i$ in (44) and substituting in (43) results in

$$\mathcal{D}(y^{\tau+1}) = \mathcal{D}(y^\tau) - \Delta t \sum_{i=1}^{N_T} b_i \mathcal{C}(\mathcal{Y}_i) + \Delta t^2 \sum_{i,j=1}^{N_T} (b_i b_j - a_{ij} b_i - a_{ji} b_j) (\mathcal{F}_i^N)^\top S \mathcal{F}_j^N.$$

For case (i), conclusion (40) follows from the fact that the matrix S is identically zero. For case (ii), since any Gauss-Legendre method satisfies the algebraic constraint

$$b_i b_j = a_{ij} b_i - a_{ji} b_j, \quad \text{for } i, j = 1, \dots, N_{GL}, \quad (45)$$

the result (40) is proven. \square

Remark 6.1. In Lemmas 5.1 and 5.2 we have characterized the conservation of the total number of particles and of the total energy by isolating the contribution associated with the flux at the boundaries of the spatial domain Ω_x . This term is associated with the presence of a source of particles or energy. Knowing the source allows one to quantify exactly the flux of particles or energy at the domain boundaries. In the case of known boundary fluxes, the last term of (27) can be computed analytically and, hence, the conservation law (28) is satisfied exactly by the fully-discrete problem under the assumptions of Theorem 6.1.

In the forthcoming subsections, we assess the capability of each family of temporal integrators of Section 3 to preserve the conservation law (26) stated in Section 5.

6.1 Conservation properties of the GL-Hermite-DG scheme

Theorem 6.1 implies that the discretization of the Vlasov-Maxwell problem with the Hermite-DG method coupled with any Gauss-Legendre method (11) yields the conservation of the number of particles and the total energy, including the contribution of the particles and energy flux at the domain boundaries, when central numerical fluxes are used in the discretization of Maxwell's equations. This is because these two quantities are linear and quadratic in y , respectively. The numerical tests in Section 7 corroborate this finding, when the implicit midpoint rule is used as temporal integrator.

The conservation of total energy in the case of upwind numerical fluxes needs to be treated separately. Indeed the total energy \mathcal{E}_{tot} does not satisfy a conservation law and can dissipate over time (depending on whether numerical dissipation dominates over the sources). As shown in Lemma 5.2, if y is the solution of (26), then

$$\frac{d\mathcal{E}_{\text{tot}}(y(t))}{dt} + \mathcal{E}_{\text{bnd}}(y(t)) \leq 0, \quad \forall y(t) \in \mathbb{R}^M, \quad (46)$$

which is a consequence of the DG spatial discretization. In the following result we show that the Gauss-Legendre methods have two properties: they preserve, at the temporal discrete level, the dissipative relation (46), and, secondly, they do not introduce any additional dissipation, in the sense that the amount of energy dissipated by the fully-discrete scheme equals the temporal approximation of the dissipative term (33) ensuing from the Hermite-DG semi-discretization.

Proposition 6.1. *Let us consider the semi-discrete problem (26) obtained with upwind numerical fluxes in the discretization of Maxwell's equations and with the initial condition $y(0)$. Let $\{y^\tau\}_{\tau=1, \dots, T/\Delta t}$ be the sequence of approximate solutions provided by the Gauss-Legendre method (11), with $y^0 = y(0)$. Then, the total energy (36) satisfies the inequality*

$$\mathcal{E}_{\text{tot}}(y^{\tau+1}) - \mathcal{E}_{\text{tot}}(y^\tau) + \Delta t \sum_{i=1}^{N_{GL}} b_i \mathcal{E}_{\text{bnd}}(\mathcal{Y}_i) \leq 0, \quad (47)$$

where $(\mathcal{Y}_i)_{i=1}^{N_{GL}}$ are defined in (11) and $(b_i)_{i=1}^{N_{GL}}$ are the weights of the Gauss-Legendre temporal scheme.

Proof. Since the total energy (36) is a quadratic function of y , as highlighted in Section 5.3, we can recast it as $\mathcal{E}_{\text{tot}}(y) = y^\top S y + \mu^\top y$, for $\mu \in \mathbb{R}^M$ and $S \in \mathbb{R}^{M \times M}$ symmetric. We can then repeat the derivation in the proof of Theorem 6.1. From (43), since any Gauss-Legendre method satisfies $b_i b_j = a_{ij} b_i - a_{ji} b_j$, we have

$$\mathcal{E}_{\text{tot}}(y^{\tau+1}) = \mathcal{E}_{\text{tot}}(y^\tau) + \Delta t \sum_{i=1}^{N_{GL}} b_i (\mu^\top + 2\mathcal{Y}_i^\top S) \mathcal{F}_i^N,$$

where $(\mathcal{Y}_i)_{i=1}^{N_{GL}}$ are defined in (11). The conclusion (47) follows by showing that

$$\sum_{i=1}^{N_{GL}} b_i (\mu^\top + 2\mathcal{Y}_i^\top S) \mathcal{F}_i^N \leq - \sum_{i=1}^{N_{GL}} b_i \mathcal{E}_{\text{bnd}}(\mathcal{Y}_i). \quad (48)$$

To prove this, we use (46) together with (26), so that

$$\begin{aligned} 0 &\geq \frac{d\mathcal{E}_{\text{tot}}(y(t))}{dt} + \mathcal{E}_{\text{bnd}}(y) = \frac{d}{dt}(y^\top S y + \mu^\top y) + \mathcal{E}_{\text{bnd}}(y) \\ &= (\mu^\top + 2y^\top S) \frac{dy}{dt} + \mathcal{E}_{\text{bnd}}(y) = (\mu^\top + 2y^\top S) \mathcal{F}^N(y) + \mathcal{E}_{\text{bnd}}(y), \quad \forall y. \end{aligned} \quad (49)$$

Taking $y = \mathcal{Y}_i$ in (49) and considering the fact that each weight b_i is non-negative, for all $i = 1, \dots, N_{GL}$ (see e.g. [24]), yields (48) and the proof is concluded. \square

To quantify the amount of local numerical dissipation associated with the GL-Hermite-DG discretization of (8), observe that, by Lemma 5.2, the quantity \mathcal{E}_{mod} in (38) defined as

$$\mathcal{E}_{\text{mod}}(y(t)) = \mathcal{E}_{\text{tot}}(y(t)) + \int_0^t (\mathcal{E}_{\text{bnd}}(y(\sigma)) + \mathcal{E}_{\text{jump}}(y(\sigma))) d\sigma,$$

is quadratic in y and satisfies (28). Applying Theorem 6.1 we can conclude that, if y^τ is the solution of the GL-Hermite-DG discretization of (8), then

$$\mathcal{E}_{\text{tot}}(y^{\tau+1}) = \mathcal{E}_{\text{tot}}(y^\tau) - \Delta t \sum_{i=1}^{N_{GL}} b_i \mathcal{E}_{\text{bnd}}(\mathcal{Y}_i) - \Delta t \sum_{i=1}^{N_{GL}} b_i \mathcal{E}_{\text{jump}}(\mathcal{Y}_i), \quad (50)$$

where $(\mathcal{Y}_i)_{i=1}^{N_{GL}}$ are defined in (11). Since the jump contribution in (50) tends to zero as the spatial and temporal meshes are refined, equation (50) entails that the total energy is asymptotically preserved and the numerical dissipation is locally bounded.

Remark 6.2. An immediate consequence of (50) is that, for the lowest order GL method, namely the implicit midpoint rule, it holds

$$\begin{aligned} \frac{\mathcal{E}_{\text{tot}}(y^{\tau+1}) - \mathcal{E}_{\text{tot}}(y^\tau)}{\Delta t} + \frac{1}{2} \sum_s m^s \int_{\partial\Omega_x} \int_{\Omega_v} (\mathbf{n} \cdot \mathbf{v}) |\mathbf{v}|^2 \left(\frac{f^{s,N,\tau+1}(\mathbf{x}, \mathbf{v}) + f^{s,N,\tau}(\mathbf{x}, \mathbf{v})}{2} \right) d\mathbf{v} dS \\ = - \left(\frac{\omega_{ce}}{\omega_{pe}} \right)^2 \sum_f \mathcal{J}_f(y^{\tau+1/2}) \leq 0. \end{aligned}$$

6.2 Conservation properties of the RK-Hermite-DG scheme

Theorem 6.1 implies that explicit Runge-Kutta schemes (10) applied to the semi-discrete Vlasov-Maxwell problem (26) conserve the number of particles. Concerning quadratic invariants, however, general explicit Runge-Kutta methods are known not to satisfy the algebraic constraint (45). This implies, in our case, that the conservation of the total energy (38) is not guaranteed by the scheme (10), not even when central numerical fluxes are used in the discretization of Maxwell's equations. This provides the motivation for the study of a modified version of the explicit Runge-Kutta methods (10) with an additional projection step that preserves the energy invariant for central numerical fluxes and maintains the semi-discrete energy dissipation (i.e., it does not add dissipation due to the time integration) for the upwind numerical fluxes. Taking the cue from the incremental direction technique [4] and relaxation RK methods [27], this task is discussed in the next subsection.

6.3 Energy-conserving explicit RK schemes

Let us consider the N_{RK} -stage explicit RK method (10) defined by the coefficients $(a_{ij})_{1 \leq j < i \leq N_{RK}}$, $(c_i)_{i=1}^{N_{RK}}$ and weights $(b_i)_{i=1}^{N_{RK}}$. We use the term *modified* Runge-Kutta scheme, to refer to the N_{RK} -stage explicit RK method having coefficients $(a_{ij})_{1 \leq j < i \leq N_{RK}}$, $(c_i)_{i=1}^{N_{RK}}$ and weights $(\hat{b}_i)_{i=1}^{N_{RK}}$, where $\hat{b}_i := \gamma^\tau b_i$

for any $1 \leq i \leq N_{RK}$. In the interval $(t^\tau, t^{\tau+1}]$, this scheme reads

$$\begin{aligned} y^{\tau+1} &= \widehat{\varphi}_{RK}(y^\tau) := y^\tau + \gamma^\tau \Delta t \sum_{i=1}^{N_{RK}} b_i \mathcal{F}^N(\mathcal{Y}_i; t^\tau + c_i \Delta t), \\ \mathcal{Y}_1 &:= y^\tau, \\ \mathcal{Y}_i &:= y^\tau + \Delta t \sum_{j=1}^{i-1} a_{ij} \mathcal{F}^N(\mathcal{Y}_j; t^\tau + c_j \Delta t), \quad i = 2, \dots, N_{RK}. \end{aligned} \tag{51}$$

The real scalar factors $\{\gamma^\tau\}_\tau$ depend on the approximate solution of the evolution problem, and are determined by imposing that a given conservation law is satisfied. Observe that, with the definition of δy^τ given in (41), we have that the standard RK scheme can be written as $\bar{y}^{\tau+1} = y^\tau + \delta y^\tau$, while the modified RK scheme reads $y^{\tau+1} = y^\tau + \gamma^\tau \delta y^\tau$ and, hence, $y^{\tau+1} = y^\tau + \gamma^\tau (\bar{y}^{\tau+1} - y^\tau)$. This implies that the modified RK scheme can be interpreted as a projection method [19, Section IV.4] that consists in projecting the current RK update onto the set of functions that satisfy the invariant constraint. Its implementation can be performed according to Algorithm 1.

Algorithm 1 Modified RK algorithm

```

1: procedure MODIFIED_RK( $y^\tau$ )
2:    $\bar{y}^{\tau+1} \leftarrow \varphi_{RK}(y^\tau)$ 
3:    $\gamma^\tau \leftarrow \text{COMPUTE\_GAMMA}(y^\tau, \bar{y}^{\tau+1})$ 
4:    $y^{\tau+1} \leftarrow y^\tau + \gamma^\tau (\bar{y}^{\tau+1} - y^\tau)$ 
5:   return  $y^{\tau+1}$ 
6: end procedure

```

In line 2 of Algorithm 1, we update the solution y^τ to the intermediate solution $\bar{y}^{\tau+1}$ by using the standard explicit RK scheme (10). In line 3 we compute the scalar factor γ^τ that is used in the projection step. In line 4 we perform the projection step obtaining the final updated solution $y^{\tau+1}$ according to (51).

In our setting, we want to ensure that the numerical solution $y^{\tau+1}$ of the modified Runge-Kutta method at time $t^{\tau+1}$ satisfies the discrete relation corresponding to (46), namely

$$\mathcal{E}_{\text{tot}}(y^{\tau+1}) - \mathcal{E}_{\text{tot}}(y^\tau) + \Delta t \sum_{i=1}^{N_{RK}} \widehat{b}_i \mathcal{E}_{\text{bnd}}(\mathcal{Y}_i) = -\varepsilon \Delta t \sum_{i=1}^{N_{RK}} \widehat{b}_i \mathcal{E}_{\text{jump}}(\mathcal{Y}_i), \tag{52}$$

with the quantities defined in (31), (32), (33) and (34), and where $\varepsilon \in \{0, 1\}$ is a user-defined coefficient that acts as follows. The choice $\varepsilon = 0$ entails that the modified RK scheme conserves the discrete energy; while the choice $\varepsilon = 1$ implies that the solution of the modified RK scheme is constrained to maintain the energy dissipation property of the semi-discrete formulation. Observe that, when central numerical fluxes are used in the discretization of Maxwell's equations (20), the term $\mathcal{E}_{\text{jump}}$ vanishes, and thus ε does not play any role.

To determine the value of the scalar factor $\gamma^\tau \in \mathbb{R}$ we impose the equality constraint associated with the energy conservation (52). For the sake of better readability, we introduce the notations

$$\delta \mathcal{E}_{\text{jump}}^{\tau, \tau+1} := \Delta t \sum_{i=1}^{N_{RK}} b_i \mathcal{E}_{\text{jump}}(\mathcal{Y}_i), \quad \delta \mathcal{E}_{\text{bnd}}^{\tau, \tau+1} := \Delta t \sum_{i=1}^{N_{RK}} b_i \mathcal{E}_{\text{bnd}}(\mathcal{Y}_i). \tag{53}$$

The following result extends to our setting the derivation of the incremental direction [4, Theorem 2.1 (i)] that guarantees energy conservation.

Theorem 6.2. Let $\{y^\tau\}_{\tau=1,\dots,T/\Delta t}$ be the sequence of numerical solutions provided by the modified RK method in (51), with $N_{RK} \geq 2$ and initial condition y^0 . Assume that the discrete total energy \mathcal{E}_{tot} and the electromagnetic energy $\mathcal{E}_{E,B}$, defined in (36) and (32), respectively, satisfy, for any τ ,

$$\left(\mathcal{E}_{\text{tot}}(\varphi_{RK}(y^\tau)) - \mathcal{E}_{\text{tot}}(y^\tau) - \mathcal{E}_{E,B}(\varphi_{RK}(y^\tau) - y^\tau) + \delta\mathcal{E}_{\text{bnd}}^{\tau,\tau+1} + \varepsilon \delta\mathcal{E}_{\text{jump}}^{\tau,\tau+1} \right) \mathcal{E}_{E,B}(\varphi_{RK}(y^\tau) - y^\tau) \neq 0, \quad (54)$$

with $\delta\mathcal{E}_{\text{bnd}}^{\tau,\tau+1}$ and $\delta\mathcal{E}_{\text{jump}}^{\tau,\tau+1}$ as in (53). Then, the conservation law (52) associated with the total energy (36) is satisfied with the choice of $\gamma^\tau \in \mathbb{R}$ given by

$$\gamma^\tau = 1 - \frac{\mathcal{E}_{\text{tot}}(\varphi_{RK}(y^\tau)) - \mathcal{E}_{\text{tot}}(y^\tau) + \delta\mathcal{E}_{\text{bnd}}^{\tau,\tau+1} + \varepsilon \delta\mathcal{E}_{\text{jump}}^{\tau,\tau+1}}{\mathcal{E}_{E,B}(\varphi_{RK}(y^\tau) - y^\tau)}, \quad \forall \tau. \quad (55)$$

Proof. Analogously to the proof of Proposition 6.1, we write the total energy (36) as $\mathcal{E}_{\text{tot}}(y) = y^\top S y + \mu^\top y$, for $\mu \in \mathbb{R}^M$ and $S \in \mathbb{R}^{M \times M}$ symmetric. Separating the kinetic and electromagnetic energy contributions, we can formally write $\mathcal{E}_{\text{kin}}(y) = \mu^\top y$ and $\mathcal{E}_{E,B}(y) = y^\top S y$. In addition, we introduce the notation $\langle a, b \rangle := a^\top S b$ for any $a, b \in \mathbb{R}^M$. The goal is to find γ^τ in (51) such that the energy conservation (52) is satisfied. With the notations introduced above, we impose

$$\mu^T y^{\tau+1} + \langle y^{\tau+1}, y^{\tau+1} \rangle - \mu^T y^\tau - \langle y^\tau, y^\tau \rangle + \gamma^\tau (\delta\mathcal{E}_{\text{bnd}}^{\tau,\tau+1} + \varepsilon \delta\mathcal{E}_{\text{jump}}^{\tau,\tau+1}) = 0.$$

Substituting expression (51) for $y^{\tau+1}$, and using the bilinearity and symmetry of the form $\langle \cdot, \cdot \rangle$, yield

$$\gamma^\tau (\mu^T \delta y^\tau + 2\langle y^\tau, \delta y^\tau \rangle + \delta\mathcal{E}_{\text{bnd}}^{\tau,\tau+1} + \varepsilon \delta\mathcal{E}_{\text{jump}}^{\tau,\tau+1}) + (\gamma^\tau)^2 \langle \delta y^\tau, \delta y^\tau \rangle = 0. \quad (56)$$

Such relation is trivially satisfied by $\gamma^\tau = 0$ corresponding to the steady state solution $y^{\tau+1} = y^\tau$, which clearly implies that the energy is the same at $t^{\tau+1}$ and t^τ . To obtain nontrivial solutions of (56), we need to assume that

$$(\mu^T \delta y^\tau + 2\langle y^\tau, \delta y^\tau \rangle + \delta\mathcal{E}_{\text{bnd}}^{\tau,\tau+1} + \varepsilon \delta\mathcal{E}_{\text{jump}}^{\tau,\tau+1}) \langle \delta y^\tau, \delta y^\tau \rangle \neq 0. \quad (57)$$

Under this condition, we obtain the nontrivial solution

$$\gamma^\tau = - \frac{\mu^T \delta y^\tau + 2\langle y^\tau, \delta y^\tau \rangle + \delta\mathcal{E}_{\text{bnd}}^{\tau,\tau+1} + \varepsilon \delta\mathcal{E}_{\text{jump}}^{\tau,\tau+1}}{\langle \delta y^\tau, \delta y^\tau \rangle}. \quad (58)$$

The proof is completed by reformulating γ^τ in terms of the discrete plasma energies. First, we note that, for $\bar{y}^{\tau+1} = \varphi_{RK}(y^\tau)$ as in Algorithm 1, it holds that

$$\langle \bar{y}^{\tau+1}, \bar{y}^{\tau+1} \rangle = \langle y^\tau, y^\tau \rangle + 2\langle y^\tau, \delta y^\tau \rangle + \langle \delta y^\tau, \delta y^\tau \rangle.$$

This allows us to rewrite the second term of the numerator of (58) as follows,

$$2\langle y^\tau, \delta y^\tau \rangle = \langle \bar{y}^{\tau+1}, \bar{y}^{\tau+1} \rangle - \langle y^\tau, y^\tau \rangle - \langle \delta y^\tau, \delta y^\tau \rangle.$$

Hence, since $\delta y^\tau = \bar{y}^{\tau+1} - y^\tau$, we have

$$\begin{aligned} \mu^T \delta y^\tau + 2\langle y^\tau, \delta y^\tau \rangle &= (\mu^T \bar{y}^{\tau+1} + \langle \bar{y}^{\tau+1}, \bar{y}^{\tau+1} \rangle) - (\mu^T y^\tau + \langle y^\tau, y^\tau \rangle) - \langle \delta y^\tau, \delta y^\tau \rangle \\ &= \mathcal{E}_{\text{tot}}(\bar{y}^{\tau+1}) - \mathcal{E}_{\text{tot}}(y^\tau) - \mathcal{E}_{E,B}(\delta y^\tau). \end{aligned}$$

Therefore, equation (58) becomes,

$$\gamma^\tau = 1 - \frac{\mathcal{E}_{\text{tot}}(\bar{y}^{\tau+1}) - \mathcal{E}_{\text{tot}}(y^\tau) + \delta\mathcal{E}_{\text{bnd}}^{\tau,\tau+1} + \varepsilon \delta\mathcal{E}_{\text{jump}}^{\tau,\tau+1}}{\mathcal{E}_{E,B}(\delta y^\tau)},$$

and condition (57) equals (54). \square

The modified method (51), (55) and Theorem 6.2 offer the discrete counterpart of the result of Lemma 5.2, for explicit temporal integrators of the Runge-Kutta family. Therefore, with the modified RK scheme, the discrete total energy is exactly conserved when central numerical fluxes are used in the DG approximation of Maxwell's equations and, hence, $\gamma^\tau = 1$. When upwind fluxes are considered, two options are possible: the discrete total energy is exactly preserved by the choice of γ^τ in (55) with $\varepsilon = 0$; or a dissipative term appears in the energy conservation equation – for $\varepsilon = 1$ – and this depends on a quadratic form of the cell interface jumps of the electromagnetic fields and is expected to go to zero with the accuracy of the DG scheme.

In the numerical implementation, Algorithm 1 is combined with Algorithm 2 that computes the scalar factor $\gamma^\tau \in \mathbb{R}$. The computation of the correction factor γ^τ in each temporal interval requires N_{RK} evaluations of the terms \mathcal{E}_{bnd} and $\mathcal{E}_{\text{jump}}$, two evaluations of the total energy at the RK update $\bar{y}^{\tau+1}$, and one evaluation of the electromagnetic energy $\mathcal{E}_{\mathbf{E},\mathbf{B}}$ at δy^τ .

Algorithm 2 Compute γ in the Maxwell solver

```

1: procedure COMPUTE_GAMMA( $y^\tau, \bar{y}^{\tau+1}$ )
2:    $\delta \mathcal{E}_{\text{jump}}^{\tau, \tau+1} \leftarrow \Delta t \sum_{i=1}^{N_{RK}} b_i \mathcal{E}_{\text{jump}}(\mathcal{Y}_i)$ 
3:    $\delta \mathcal{E}_{\text{bnd}}^{\tau, \tau+1} \leftarrow \Delta t \sum_{i=1}^{N_{RK}} b_i \mathcal{E}_{\text{bnd}}(\mathcal{Y}_i)$ 
4:    $\gamma^\tau \leftarrow 1 - \frac{\mathcal{E}_{\text{tot}}(\bar{y}^{\tau+1}) - \mathcal{E}_{\text{tot}}(y^\tau) + \delta \mathcal{E}_{\text{bnd}}^{\tau, \tau+1} + \varepsilon \delta \mathcal{E}_{\text{jump}}^{\tau, \tau+1}}{\mathcal{E}_{\mathbf{E},\mathbf{B}}(\bar{y}^{\tau+1} - y^\tau)}$ 
5: end procedure

```

Remark 6.3 (Explicit Euler scheme). For the lowest order RK scheme (10), namely explicit Euler method, the result of Theorem 6.2 does not apply. This is due to the fact that condition (54) is not satisfied. Indeed, in the explicit Euler scheme, $\delta y^\tau = \Delta t \mathcal{F}^N(y^\tau)$ in (41) and $\delta \mathcal{E}_{\text{bnd}}^{\tau, \tau+1} + \delta \mathcal{E}_{\text{jump}}^{\tau, \tau+1} = \Delta t (\mathcal{E}_{\text{bnd}}(y^\tau) + \mathcal{E}_{\text{jump}}(y^\tau))$ in (53). Hence, the first factor in condition (57) reads

$$\Delta t (\mu^T \mathcal{F}^N(y^\tau) + 2 \langle y^\tau, \mathcal{F}^N(y^\tau) \rangle + \mathcal{E}_{\text{bnd}}(y^\tau) + \varepsilon \mathcal{E}_{\text{jump}}(y^\tau)). \quad (59)$$

In view of Lemma 5.2, the total energy $\mathcal{E}_{\text{tot}}(y) = \mu^T y + \langle y, y \rangle$ satisfies, for any $y \in \mathbb{R}^M$, equation (44) with $\mathcal{D} = \mathcal{E}_{\text{tot}}$ and $\mathcal{C} = \mathcal{E}_{\text{bnd}} + \varepsilon \mathcal{E}_{\text{jump}}$. This implies that

$$-\mathcal{E}_{\text{bnd}}(y^\tau) - \varepsilon \mathcal{E}_{\text{jump}}(y^\tau) = \mu^T \mathcal{F}^N(y^\tau) + 2 \langle y^\tau, \mathcal{F}^N(y^\tau) \rangle.$$

Hence, the term in (59) vanishes and condition (57) cannot be satisfied.

Remark 6.4. The modified Runge-Kutta method (51) preserves linear conservation laws according to Theorem 6.1. Indeed, the modified scheme can still be expressed as linear combinations of explicit Euler steps, since it is an explicit RK method of the family (10) with weights $(\gamma^\tau b_i)_{i=1}^{N_{RK}}$ for any τ .

As proven in [4, Theorem 2.1 (ii)] the projection step introduced by the modified RK method causes the loss of one order of convergence if compared with the standard RK scheme. However, if the numerical solution of the modified RK method at step $\tau + 1$ is interpreted as an approximation of the exact solution at time $t^\tau + \gamma^\tau \Delta t$ the accuracy of the base scheme is recovered [27, Theorem 2.7 and Corollary 2.10]. In the following result we show that our specific γ^τ , defined in (55), satisfies the condition $\gamma^\tau = 1 + \mathcal{O}(\Delta t^{p-1})$ for $\Delta t \rightarrow 0$.

Proposition 6.2. *Consider an explicit RK scheme (10) of order $p \geq 2$ for the numerical approximation of (26). Let $\{y^\tau\}_{\tau=1, \dots, T/\Delta t}$ be the sequence of numerical solutions of (26) obtained with the modified RK method (51) with initial condition $y^0 = y(0)$ and γ^τ defined as in (55). Under the assumptions of Theorem 6.2, if $\mathcal{E}_{\mathbf{E},\mathbf{B}}(y^\tau) \neq 0$ for all τ , the modified RK scheme has order of accuracy*

(i) $p - 1$, if the numerical solution $y^{\tau+1}$ is interpreted as an approximation of $y(t^\tau + \Delta t)$;

(ii) p , if the numerical solution $y^{\tau+1}$ is interpreted as an approximation of $y(t^\tau + \gamma^\tau \Delta t)$.

Proof. For the sake of better readability, in the following derivation, we use the notation $\mathcal{E} := \mathcal{E}_{\text{bnd}} + \varepsilon \mathcal{E}_{\text{jump}}$ and $\delta \mathcal{E}^{\tau, \tau+1} := \delta \mathcal{E}_{\text{bnd}}^{\tau, \tau+1} + \varepsilon \delta \mathcal{E}_{\text{jump}}^{\tau, \tau+1}$. Since the RK method φ_{RK} is of order p , it can be written as

$$\bar{y}^{\tau+1} = \varphi_{RK}(y^\tau) = y(t^{\tau+1}) + e^{\tau+1}, \quad (60)$$

where $e^{\tau+1} := C \Delta t^{p+1} + O(\Delta t^{p+2})$, $C \in \mathbb{R}^M$, and $y(t^{\tau+1})$ is the exact solution, at time $t^{\tau+1}$, of

$$\begin{cases} y'(t) = \mathcal{F}^N(y(t); t), & \text{in } (t^\tau, t^{\tau+1}], \\ y(t^\tau) = y^\tau. \end{cases}$$

The exact solution satisfies the conservation law (37) so that

$$\mathcal{E}_{\text{tot}}(y(t^{\tau+1})) - \mathcal{E}_{\text{tot}}(y^\tau) + \int_{t^\tau}^{t^{\tau+1}} \mathcal{E}(y(t)) dt = 0.$$

Exploiting this conservation law and equation (60), the numerator in the expression of γ^τ in (55) can be written as

$$\begin{aligned} \mathcal{E}_{\text{tot}}(\varphi_{RK}(y^\tau)) - \mathcal{E}_{\text{tot}}(y^\tau) + \delta \mathcal{E}^{\tau, \tau+1} &= \mu^\top e^{\tau+1} + \langle e^{\tau+1}, e^{\tau+1} \rangle + 2 \langle y(t^{\tau+1}), e^{\tau+1} \rangle \\ &\quad + \Delta t \sum_{i=1}^{N_{RK}} b_i \mathcal{E}(\mathcal{Y}_i) - \int_{t^\tau}^{t^{\tau+1}} \mathcal{E}(y(t)) dt \\ &= \Delta t^{p+1} (\mu^\top C + \langle y^\tau, C \rangle) + e_q^{\tau+1} + O(\Delta t^{p+2}), \end{aligned} \quad (61)$$

where $e_q^{\tau+1}$ is the quadrature error introduced by the approximation $\delta \mathcal{E}^{\tau, \tau+1}$ in (53). By means of Taylor expansions, it can be shown that the quadrature error has the order of the corresponding RK method, namely, for some $c = c(\mathcal{E}) \in \mathbb{R}$,

$$\left| \int_{t^\tau}^{t^{\tau+1}} \mathcal{E}(y(t)) dt - \Delta t \sum_{i=1}^{N_{RK}} b_i \mathcal{E}(\mathcal{Y}_i) \right| \approx c \Delta t^{p+1} + O(\Delta t^{p+2}).$$

Moreover, the denominator of γ^τ in (55) can be expanded using Taylor expansions and gives

$$\begin{aligned} \mathcal{E}_{E,B}(\varphi_{RK}(y^\tau) - y^\tau) &= \langle y(t^{\tau+1}) - y^\tau + e^{\tau+1}, y(t^{\tau+1}) - y^\tau + e^{\tau+1} \rangle \\ &= \Delta t^2 \langle \frac{dy}{dt}(y^\tau), \frac{dy}{dt}(y^\tau) \rangle + O(\Delta t^3) = \Delta t^2 \mathcal{E}_{E,B}(y^\tau) + O(\Delta t^3). \end{aligned} \quad (62)$$

Combining (61) with (62), it follows that $\gamma^\tau = 1 + \Delta t^{p-1}$ for $\Delta t \rightarrow 0$.

The conclusion follows from the fact that

$$\begin{aligned} y^{\tau+1} &= \varphi_{RK}(y^\tau) + (\gamma^\tau - 1)(\varphi_{RK}(y^\tau) - y^\tau) \\ &= y(t^{\tau+1}) + O(\Delta t^{p+1}) + (\gamma^\tau - 1)(y(t^{\tau+1}) - y^\tau + O(\Delta t^{p+1})). \end{aligned}$$

Taylor expansion of $y(t^\tau)$ around $t^{\tau+1}$ yields

$$y^{\tau+1} = y(t^{\tau+1}) + O(\Delta t^{p+1}) + (\gamma^\tau - 1) \Delta t y'(t^{\tau+1}) + O((\gamma^\tau - 1) \Delta t^2). \quad (63)$$

We consider the two cases (i) and (ii) separately and use the fact that $\gamma^\tau = 1 + O(\Delta t^{p-1})$.

(i) Eq. (63) yields

$$y^{\tau+1} - y(t^{\tau+1}) = O(\Delta t^p).$$

(ii) Taylor expansion of $y(t^\tau + \gamma^\tau \Delta t) = y(t^{\tau+1} + (1 - \gamma^\tau) \Delta t)$ around $t^{\tau+1}$, together with Eq. (63), yields

$$y^{\tau+1} - y(t^\tau + \gamma^\tau \Delta t) = O(\Delta t^{p+1}).$$

□

7 Numerical experiments

In this section, we investigate and assess the conservation properties of the numerical methods discussed in the previous sections. We test seven variants, which differ for the temporal integration algorithm and the numerical flux in the discretization of Maxwell’s equations. We denote them with the abbreviations reported in Table 1.

IMC	—	Implicit Midpoint rule with Central flux
IMU	—	Implicit Midpoint rule with Upwind flux
RKC	—	Explicit Runge-Kutta with Central flux
RKU	—	Explicit Runge-Kutta with Upwind flux
MRKC	—	Modified explicit Runge-Kutta with Central flux
MRKU0	—	Modified explicit Runge-Kutta with Upwind flux with $\varepsilon = 0$
MRKU1	—	Modified explicit Runge-Kutta with Upwind flux with $\varepsilon = 1$

Table 1: Abbreviations for the numerical methods used in the numerical tests. The term ‘explicit Runge-Kutta’ refers to the non-adaptive third order Runge-Kutta method of Bogacki and Shampine [2].

Some of the numerical methods tested in this section are implicit schemes; therefore, they require the solution of large nonlinear systems of equations at each time step. A practical implementation requires efficient nonlinear solvers coupled with preconditioned iterative linear solvers. We leave the development of efficient implementations of implicit temporal integrators to future work. In all tests that use implicit time integration, nonlinear systems were solved with an unpreconditioned Jacobian-Free-Newton-Krylov (JFNK) method with relative tolerance of 10^{-8} and absolute tolerance of 10^{-50} . The Krylov linear solver that is embedded in the JFNK method is the generalized minimum residual (GMRES) method with relative tolerance of 10^{-5} and absolute tolerance of 10^{-50} .

The development of finer and finer scales in velocity space is a common phenomenon in collisionless plasmas, known as filamentation. In a spectral discretization, this implies that higher order spectral modes are progressively excited until recurrence effects develop when the velocity-space structures reach scales that are no longer resolved by the truncated Hermite expansion [6, 25]. An artificial collisional operator can then be employed to prevent recurrence by damping high order modes. This collisional operator must always be used in a convergence sense, without significantly affecting the collisionless physics of interest. We adopt here the same collisional operator introduced in Ref. [10], by adding to the operator \mathcal{A} in (17a) the term $\mathcal{C}(f^{s,N}) = \nu \nabla_v \cdot (\mathbf{v} f^{s,N} + \frac{1}{2} \nabla_v f^{s,N})$, where $\nu > 0$ is the collision rate, tested against any pair of functions $(\Psi, \varphi) \in \tilde{\mathcal{H}}^N \times \mathcal{V}^N$. When $\Psi = \Psi^{n,m,p}(\boldsymbol{\xi}^s)$ and $\varphi = \varphi^{I,l}(\mathbf{x})$, as defined in Section 4, then the collisional term reads

$$\nu [\kappa_x^{-1} n(n-1)(n-2) + \kappa_y^{-1} m(m-1)(m-2) + \kappa_z^{-1} p(p-1)(p-2)] C_{n,m,p}^{s,I,l}(t), \quad (64)$$

where $\kappa_\beta = N_{v_\beta}(N_{v_\beta} - 1)(N_{v_\beta} - 2)$ for all $\beta \in \{x, y, z\}$. Since the proposed collisional operator does not directly act on the first three Hermite modes, it does not affect the conservation of total mass, momentum and energy [10].

7.1 Whistler instability

We start with the whistler instability test, where an electromagnetic whistler wave grows from an unstable particle distribution function with different temperatures along and perpendicular to the background magnetic field, see e.g. [14]. In collisionless plasmas, the whistler instability grows due to a gyroresonance between a small part of the electron population and the wave. As such, this problem represents a rather sensitive test of the model’s ability to capture kinetic effects. In this test, we consider two different time steps $\Delta t = 0.01$ and 0.005 , and DG polynomial spaces of degree $N_{DG} = 1$ (linear) and 2 (quadratic). All other numerical parameters and the initial condition are fixed and are outlined below. The computational domain of the physical space is reduced to one dimension ($N_y = N_z = 1$), with $\Omega_x = [0, 2\pi]$ partitioned into a uniform grid with $N_x = 72$ elements. Periodic boundary conditions

are considered. For the numerical approximation in velocity, we use 10 Hermite basis function in each direction (i.e. $N_{v_x} = N_{v_y} = N_{v_z} = 9$). Further, for the initial configuration we consider the magnetic field $B_x = 1$, while the distribution functions for electrons and protons (ions) are Maxwellian distributions with uniform density. Moreover, we set $\alpha_\beta^s = \sqrt{2}v_{T_\beta^s}$, and $u_\beta^s = 0$ for $\beta \in \{x, y, z\}$ and $s \in \{e, i\}$. We use a realistic ion-to-electron mass ratio $m_i/m_e = 1836$, thermal velocities $v_{T_\beta^e} = v_{T_\beta^i} \sqrt{m_i/m_e} = 0.125$ for $\beta \in \{y, z\}$ with the exception of the reduced electron thermal velocity along the x -axis, $v_{T_x^e} = v_{T_x^i} \sqrt{m_i/m_e} = 0.056$, to create an anisotropic distribution function which is the source of the instability. The electron plasma/gyrofrequency ratio is $\omega_{pe}/\omega_{ce} = 4$, and the collisional rate in (64) is $\nu = 1$. In order to seed the whistler instability, we initialize a small electron current perturbation in the x -direction, $j_x^e(\mathbf{x}) = 10^{-3} \cos(x)$, by exciting the Hermite mode $C_{1,0,0}^e$ in (14).

Before proceeding to the numerical study of the conservation properties, we assess the capability of all considered methods to reproduce the correct physical results, in particular, the exponential growth of the electromagnetic whistler wave with the theoretically predicted growth rate from an initial small perturbation. It is sufficient to monitor the time evolution of the first Fourier mode of the magnetic field $\hat{B}_z(k)$, with $k = 1$, and

$$\hat{B}_z(k) = \sum_I B_z(x_c^I) e^{ikx_c^I}, \quad (65)$$

where x_c^I is the center of the I -th DG cell. Most of the considered methods produce a visually indistinguishable evolution of $\hat{B}_z(1)$, matching the theoretically predicted growth rate $\gamma = 0.035$. This has been labeled as 'Reference' solution in Fig. 2 (the only tests which visually deviate from reference curve are discussed below). However, the method MRKU0 with $N_{DG} = 1$ exhibits a noticeable deviation from the reference solution, independent of the time step, as shown in Figure 2. Increasing the spatial accuracy of MRKU0 by means of higher order DG polynomials, $N_{DG} = 2$, makes it consistent with the other methods and produces a curve that is visually indistinguishable from the reference curve in Fig. 2. It is interesting to note that, on this example, MRKU0 (where energy conservation is imposed exactly) is actually not as accurate as MRKU1 (which respects the energy dissipation introduced by upwind fluxes in Maxwell's equations). We will further comment on this behavior at the end of Section 7.2.

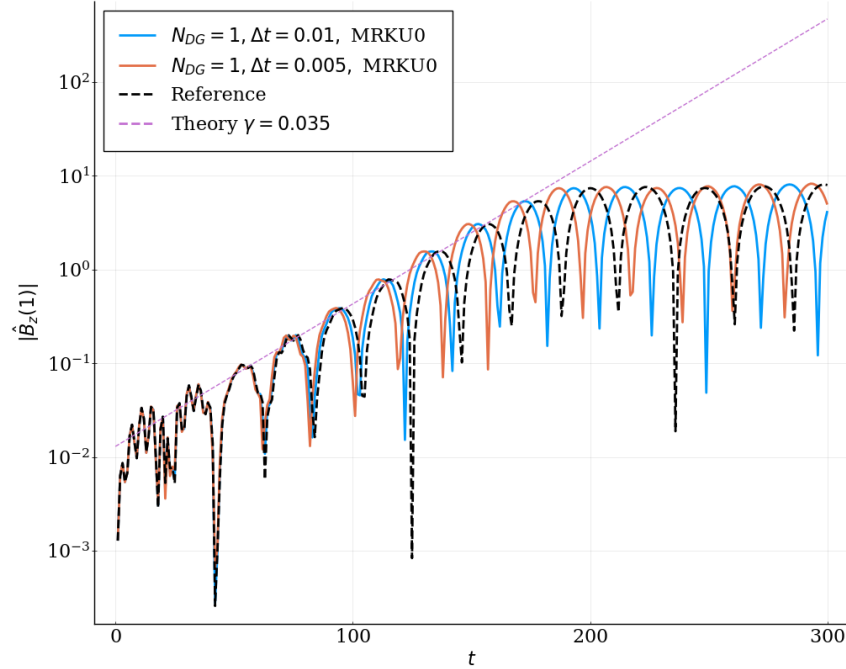


Figure 2: Whistler instability benchmark: time evolution of $|\hat{B}_z(1)|$. The numerical results show spatial accuracy deterioration for the MRKU0 method with $N_{DG} = 1$, unlike all other tested methods (reference).

All tested methods conserve the number of particles: Explicit methods (RKC, RKU, MRKC, MRKU0, MRKU1) up to machine precision, while implicit methods (IMC, IMU) with error bound by the tolerance of the nonlinear solver and independent of the space-time resolution (i.e., Δt , N_{DG}). In Fig. 3 we report the evolution of the relative error in the number of electrons with respect to the initial value for two methods, RKC and IMC with $N_{DG} = 1$ and $\Delta t = 0.01$.

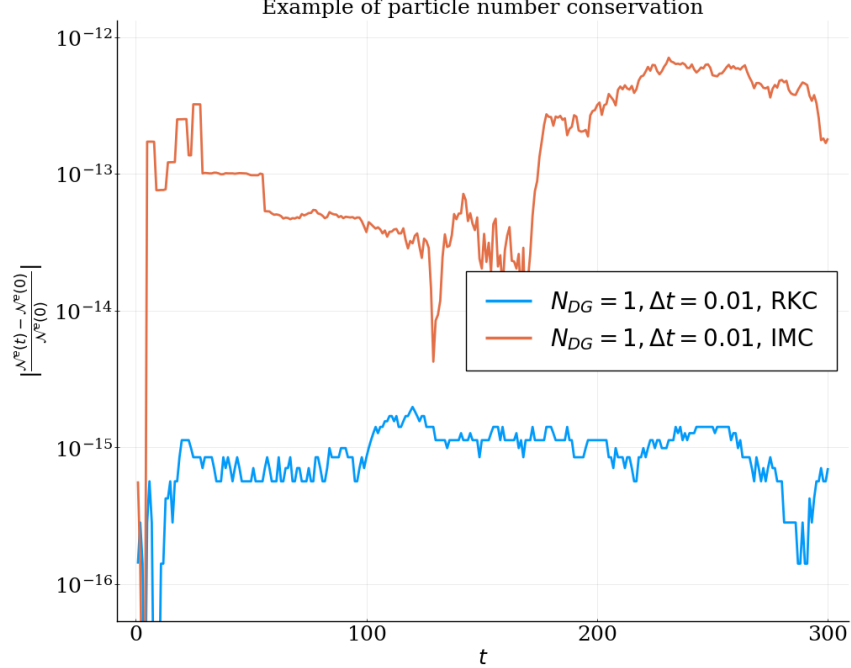


Figure 3: Whistler instability benchmark: time evolution of the error in the number of electrons for RKC and IMC with $N_{DG} = 1$ and $\Delta t = 0.01$.

In the numerical study of the energy conservation properties of the proposed methods, we first consider the family of methods where central fluxes are used in the spatial approximation of Maxwell’s equations, i.e., IMC, RKC, and MRKC. Note that, under this assumption, the energy flux at the mesh interfaces $\mathcal{E}_{\text{jump}}$ in (33) vanishes. In Fig. 4 we report the evolution of the error in the total energy, defined in Eq. (36), for different temporal integrators. In the left panel, the IMC method is studied for different temporal and spatial resolutions: as expected, all runs show bounded errors with magnitude of the order of the nonlinear solver tolerance. Next, the energy error of the RKC method (middle panel) depends on the temporal approximation, and is completely independent of the spatial resolution (curves with different N_{DG} , but with identical time step, coincide). Moreover, curves with different time step ($\Delta t = 0.01$ and 0.005) differ by a factor of $\sim 2^3 = 8$ (marked as a black two sided arrow), which is consistent with the third order of the Runge-Kutta method in use. The right panel in Fig. 4 shows the error in the conservation of total energy associated with the MRKC scheme. In this case, the error in energy conservation is maintained around machine precision², with a small dependence on temporal and spatial resolutions.

²Here and throughout this section, “machine precision” is used to describe anything from 10^{-15} to 10^{-13} .

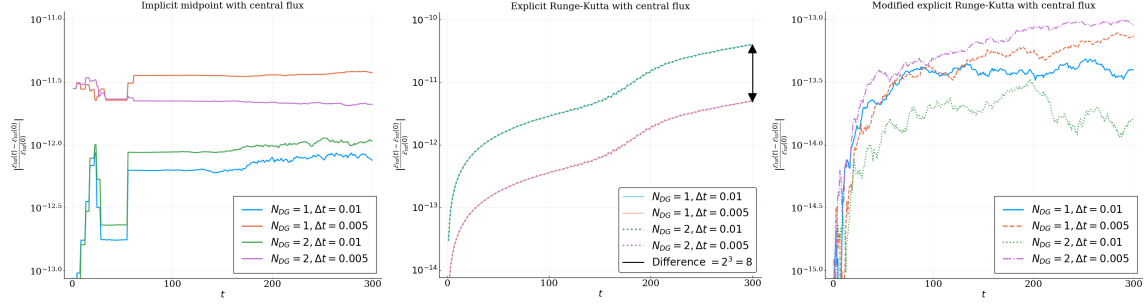


Figure 4: Whistler instability benchmark: time evolution of the relative error in the conservation of the total energy for IMC (left), RKC (middle), and MRKC (right) methods, and for different spatial and temporal resolutions.

Finally, we consider the error in the conservation of the total energy when upwind fluxes are employed in the spatial approximation of Maxwell's equations. The numerical results are presented in Fig. 5 and corroborate the findings of Theorem 6.2. The MRKU0 method ensures conservation of the total energy to machine precision and this is fairly independent of the space-time resolution, as shown in the left panel of Fig. 5. All the other upwind methods, i.e., IMU, RKU, MRKU1, dissipate energy: for completeness of exposition, we report, in the middle and right panels of Fig. 5, the absolute value of the error in the conservation of the total energy. The spatial polynomial degree is $N_{DG} = 1$ for the results shown in the middle panel, while $N_{DG} = 2$ for the results in the right panel. Note that the quantity shown in the middle and right panels of Fig. 5 is related to the discrete energy flux at the mesh interfaces, namely, the right hand side of Eq. (37). The value of this quantity depends on both the temporal discretization and the spatial approximation. For $N_{DG} = 1$ and sufficiently small time step, the error is independent of the temporal integrator of choice and is dominated by the spatial discretization error (middle panel). For $N_{DG} = 2$ (right panel), the energy error has a very small magnitude (less than $\sim 10^{-12}$) until around $t = 100$. Before this time, we record different behaviors for different temporal integrators. The error for MRKU1 is around machine precision with a rather negligible dependence on Δt . The error for IMU is generally higher and is determined by the tolerance of the nonlinear solver (as determined by different runs with the same parameters but a lower tolerance of the nonlinear solver, not shown). Finally, we can see that the traditional Runge-Kutta scheme RKU performs rather well in this test case, with the error on the total energy remaining comparable to that for IMU. RKU also shows the expected third order scaling of the algorithm with respect to Δt . For times $t > 150$, all curves converge to the same behavior, signaling that the spatial discretization error is now dominant. This is consistent with Eq. (36), which shows that the variation of the total energy accumulates in time by summing the negative-definite contributions coming from the spatial discretization.

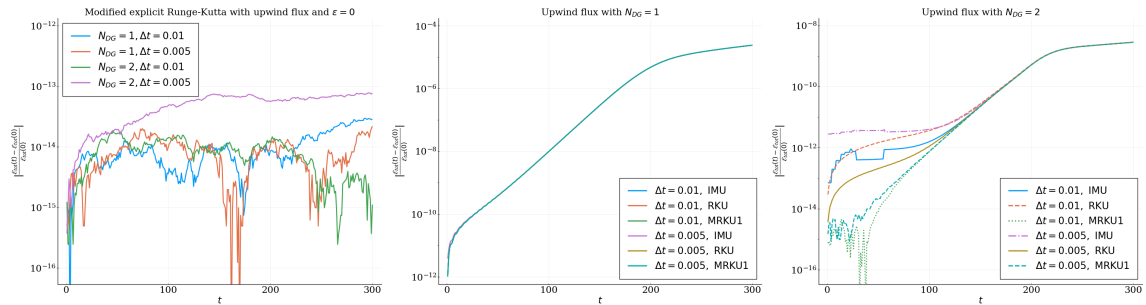


Figure 5: Whistler instability benchmark: time evolution of the relative error in the conservation of the total energy for MRKU0 (left), IMU, RKU, MRKU1 with $N_{DG} = 1$ (middle), and IMU, RKU, MRKU1 with $N_{DG} = 2$ (right), for different time steps.

We note that nonlinear evolution of the whistler instability may in principle result in development of strong non-Maxwellian features in the distribution function. Depending on the spectrum and the

saturation amplitude of the excited modes under a given set of conditions, such departures may pose challenges to a method that uses a small number of Hermite modes and applies strong damping to high-order moments. The growth rate and the saturation amplitude of the solution presented in this section were checked for convergence with respect to the number of Hermite polynomials by performing additional simulations with 20 Hermite basis functions in each direction and varying collisionality. The solution was found to be fully converged with respect to the number of Hermite polynomials, while reducing the collisionality by almost an order of magnitude resulted in saturation amplitude changing by 7.5% and a phase shift of the oscillations in saturated state, which is inconsequential in most practical applications.

7.2 High frequency electromagnetic waves

From the results presented above, it may be tempting to conclude that using the central fluxes in the approximation of Maxwell's equations is preferable in practice, given their energy conservation properties and the fact that enforcing energy conservation in upwind-based methods leads to a degradation of accuracy. However, methods based on upwind fluxes may be preferable in some situations, in particular because they tend to reproduce the physical dispersion properties of plasma waves in a better way compared to the central-flux counterparts [23, 37].

In this section, we illustrate the difference between central and upwind fluxes in resolving the dispersion properties of X mode waves in the cold-plasma limit. In the simplest case, an X mode is an electromagnetic electron wave (the ions remain essentially static) with wave vector and wave electric field perpendicular to the background magnetic field.

In this test, we use a one dimensional ($N_y = N_z = 1$) spatial domain $\Omega_x = [0, 100\pi]$ with $N_x = 500$, periodic boundary conditions, and linear DG polynomials $N_{DG} = 1$. We consider the temporal interval $[0, 100\pi]$ with time step $\Delta t = \pi/25$. Since treating the plasma as a fluid is sufficient for this test, we use only 4 Hermite polynomials per velocity direction. Further, the background magnetic field is initialized to $B_z = 1$, and the distribution function for the electrons is Maxwellian. Ions constitute a static background. Moreover, we set $\alpha_\beta^e = 0.002$, and $u_\beta^e = 0$ for $\beta \in \{x, y, z\}$. The electron plasma/gyrofrequency ratio is $\omega_{pe}/\omega_{ce} = 1$ and no artificial collisionality is used ($\nu = 0$). We perturb the initial electron current so that

$$j_y^e(\mathbf{x}) = 10^{-4} \exp\left(-\left(\frac{x - L_x/2}{0.15L_x}\right)^2\right) \sum_{i=1}^4 A_i \sin(k_i x + \Phi_i), \quad (66)$$

with $k_i = 50ik_{\min}$, for $i \in \{1, 2, 3, 4\}$ and $k_{\min} = 2\pi/L_x$, $A_i \in \{0.598, 0.517, 0.193, 0.218\}$, $\Phi_i \in \{0.305, 0.586, 0.050, 0.089\}$.

The top left panel of Fig. 6 shows the relative error in the conservation of the total energy (the normalization factor $\mathcal{E}_{tot}(0)$ includes the energy of the background magnetic field) for all methods summarized in Table 1. Similar considerations as for the whistler instability can be made, with the exception that this test does not have any instability, so the excited waves remain of small amplitude. The relative energy error is thus small for all methods. In summary, the MRKC and MRKU0 methods conserve energy up to machine precision, IMC conserves energy up to a level determined by the tolerance of the nonlinear solver, the energy error in RKC is quite small and depends on the accuracy of the temporal discretization (as demonstrated by additional runs with different values of Δt but all other parameters unchanged, not shown) and IMU, RKU, and MRKU1 dissipate energy as expected. Note that the energy errors for RKU and MRKU1 are very similar, suggesting that the RK correction in the upwind-based scheme is not so important for this example.

In order to diagnose the dispersion properties of the X mode waves, we plot the spectrum of the electric field E_y computed with the discrete Fourier transform, namely

$$\hat{E}_y(\omega, k) = \sum_{n, I} E_y(x_c^I, t_n) e^{i\omega t_n} e^{ikx_c^I} H_n, \quad (67)$$

where $t_n = n\Delta t$, x_c^I is the center of I -th DG cell, and $H_n = \sin^2(\pi n/N_t)$ is a Hann time window applied to the data to reduce potential artifacts of the Fourier transform originating from non-periodic time

signals, N_t is a number of time steps. The logarithm of the absolute value of \hat{E}_y in (67) is shown in Fig. 6 and in Fig. 7, for the numerical methods using central and upwind fluxes, respectively. The theoretical dispersion relation for the X mode (lower and upper branches) is plotted with a gray dashed line, the resonance frequency ω_{UH} (the upper hybrid frequency) with a green dashed line, and the cut-off frequencies ω_R and ω_L with red and blue dashed lines, respectively. All methods resolve the lower frequency branch ($\omega_L < \omega < \omega_{UH}$) satisfactorily. By contrast, differences can be observed in the resolution of the high frequency branch ($\omega > \omega_R$). First, high frequency waves which are spatially well-resolved, i.e., with $k < 2.5$ (more than 4 DG cells per wavelength) are well captured in both upwind- and central-based methods. However, poorly resolved modes $k > 2.5$ (less than 4 DG cells per wavelength) are mostly suppressed in upwind-based methods, while they are still present in central-based methods. This may be attributed to dissipation in upwind methods suppressing the unresolved modes and making the methods generally more stable. We also note that the implicit methods (IMC and IMU) are more noisy for this example: all wavenumbers are excited to amplitudes that are small but visible on the logarithmic-scale plot by the fact that the nonlinear system converges only up to the relatively high tolerance of the nonlinear solver considered here. However, the IMU method suppresses most of this noise by intrinsic dissipation, as one can see by comparing with the spectrum of IMC. Additionally, the MRKU0 method exhibits numerous unphysical modes in the spectrum, particularly for higher frequencies ω .

Overall, this example shows a case where upwind fluxes in Maxwell's equations might be preferable to central fluxes to avoid high-frequency modes that are not resolved by the mesh. It also confirms that forcing the exact conservation of the total energy in the explicit upwind scheme (MRKU0) might lead to a lack of accuracy of the overall simulation. This behavior, also observed in the whistler instability test, can be interpreted as caused by an erroneous energy redistribution in space or, more precisely, spectrally. We believe that the projection step, which is only aware of the temporal discretization, can properly correct energy errors which come from the Runge-Kutta step, but not due to the spatial discretization. Methods based on upwind fluxes in Maxwell's equations damp poorly resolved modes with $k \sim \Delta x^{-1}$ featuring additional stability guarantees compared to methods based on central fluxes (cf. Figure 6 vs. Figure 7). This damping of the energy has magnitude that depends on the spatial resolution. If one tries to compensate this damping by a projection during the Runge-Kutta time step (as in MRKU0), the excessive energy is deposited to other modes and this leads to accuracy loss. On the other hand, accuracy can be retained in case of upwind fluxes when the upwind damping is retained, i.e., in MRKU1, or when the damping is absent, i.e., in methods based on central fluxes.

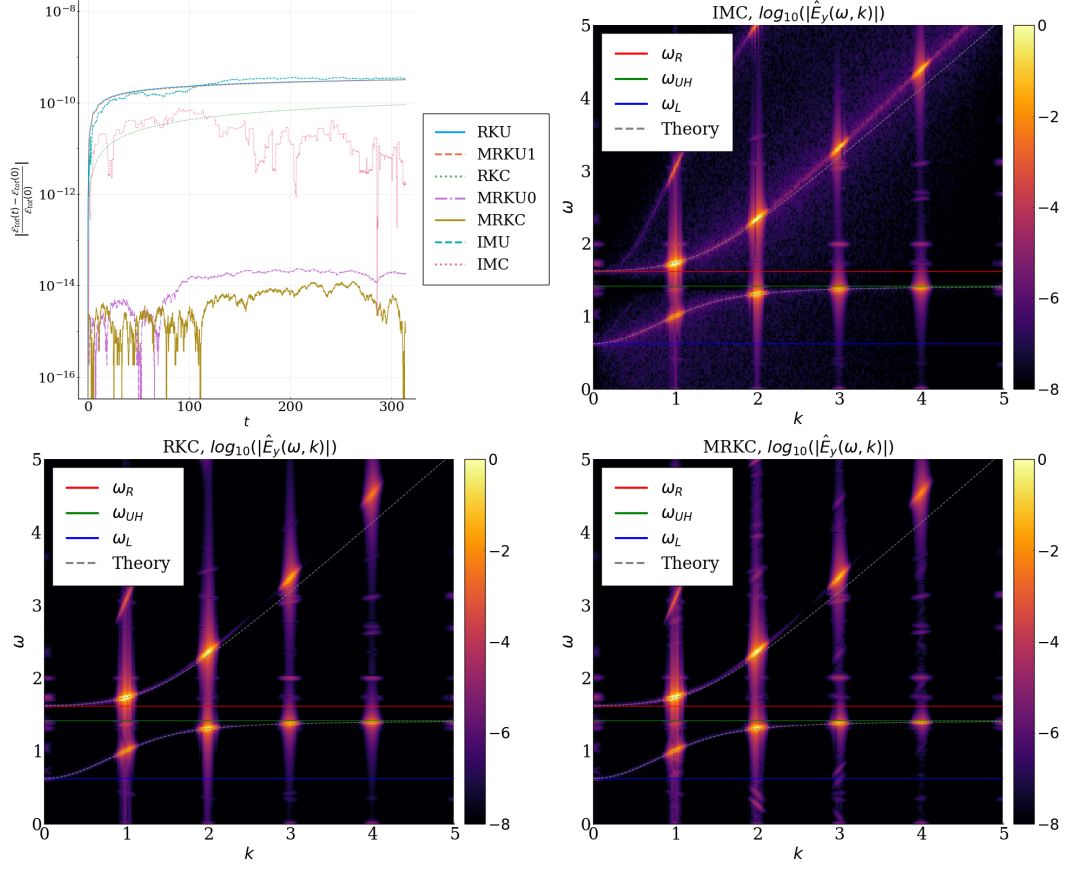


Figure 6: X mode test: relative error in the conservation of the total energy (top left); wave spectrum computed from $E_y(\mathbf{x}, t)$ for methods with central fluxes, i.e., IMC (top right), RKC (bottom left), and MRKC (bottom right).

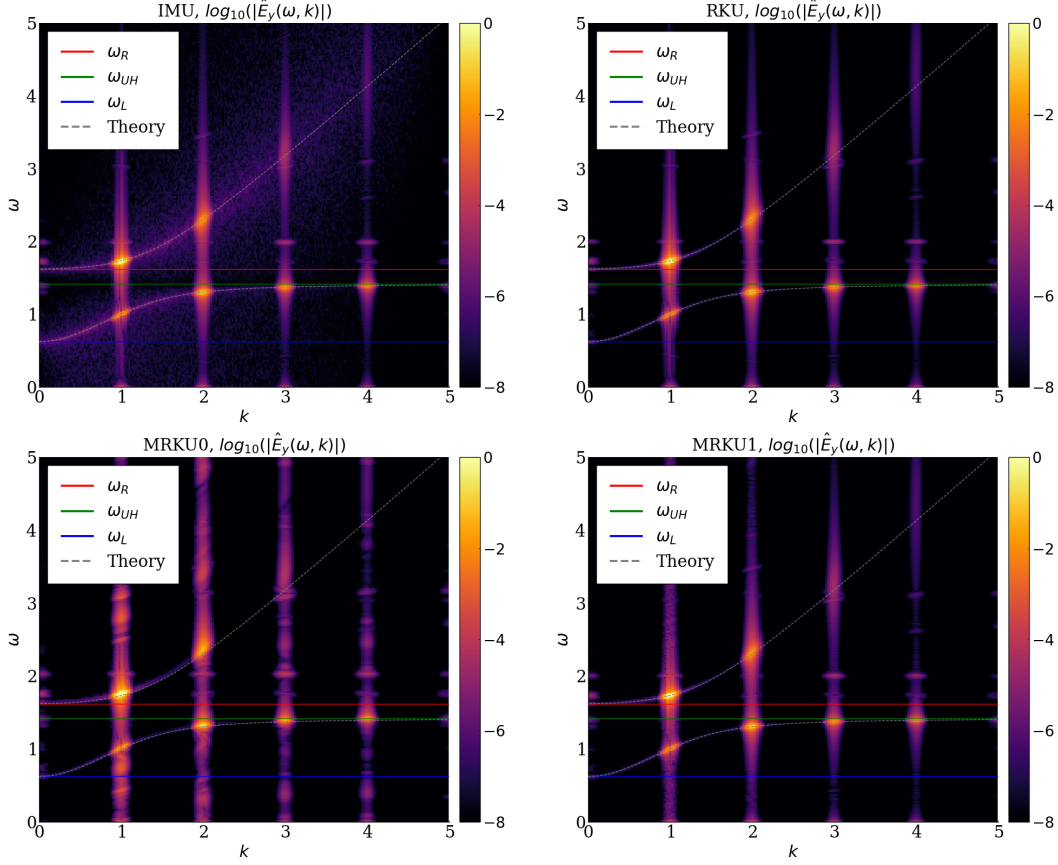


Figure 7: X mode test: wave spectrum computed from $E_y(\mathbf{x}, t)$ for methods with upwind fluxes, i.e., IMU (top left), RKU (top right), MRKU0 (bottom left), and MRKU1 (bottom right).

7.3 Orszag-Tang vortex

In the last test, we investigate the performance of the proposed methods in conserving the total energy when solving the Orszag-Tang vortex problem. In the Orszag-Tang vortex problem [35], two large-scale vortices are initialized and evolve by forming smaller and smaller current sheets and other filamentary structures. In collisionless plasma, the Orszag-Tang initial conditions lead to development of turbulence via breaking (reconnection) of the current sheet formed by the initial evolution [see e.g. 36]. The overall energy dissipation in such a case is thought to be dominated by kinetic effects that become significant at small scales [see e.g. 40, and references therein]. Therefore, this test is an example of the complex, multi-scale problem involving transition between the large-scale, fluid-like behavior of the plasma and the small-scale, dissipative processes involving kinetic physics.

We consider temporal and spatial discretizations with different resolutions: in particular, the time steps $\Delta t \in \{0.05, 0.025\}$, and DG polynomial spaces $N_{DG} = 1$ (linear) and $N_{DG} = 2$ (quadratic). All other numerical parameters and initial conditions are fixed and are outlined below. The computational domain in physical space is two dimensional ($N_z = 1$) with $\Omega_x = [0, L_x] \times [0, L_y]$, $L_x = L_y = 50$, and periodic boundary conditions. It is discretized with a uniform grid with $N_x = N_y = 108$ elements. We set $N_{v_x} = N_{v_y} = N_{v_z} = 3$ for the velocity Hermite expansion. The initial magnetic field is set to

$$\begin{aligned} B_x(\mathbf{x}) &= -\delta B \sin(k_y y + 4.1), \\ B_y(\mathbf{x}) &= \delta B \sin(2k_x x + 2.3), \\ B_z(\mathbf{x}) &= 1, \end{aligned}$$

with $\delta B = 0.2$, $k_x = 2\pi/L_x$, $k_y = 2\pi/L_y$. The values 4.1 and 2.3 are arbitrary phases that remove any artificial symmetry in the initial setup. The distribution functions for electrons and ions are initialized

to be shifted Maxwellian distributions with spatially uniform density (species superscripts are omitted for clarity),

$$f(\mathbf{x}, \mathbf{v}, t) = \prod_{\beta \in \{x, y, z\}} \frac{1}{v_{T\beta} \sqrt{2\pi}} \exp \left[-\frac{(v_\beta - U_\beta(\mathbf{x}))^2}{2v_{T\beta}^2} \right],$$

with electron and ion velocities

$$\begin{aligned} U_x^e(\mathbf{x}) &= U_x^i(\mathbf{x}) = -\delta B v_a \sin(k_y y + 0.5), \\ U_y^e(\mathbf{x}) &= U_y^i(\mathbf{x}) = \delta B v_a \sin(k_x x + 1.4), \\ U_z^e(\mathbf{x}) &= -\frac{\delta B \omega_{ce}}{\omega_{pe}} (2k_x \cos(2k_x x + 2.3) + k_y \cos(k_y y + 4.1)), \\ U_z^i(\mathbf{x}) &= 0, \end{aligned}$$

where $v_a = 0.1$ and $\omega_{pe}/\omega_{ce} = 2$. The values 0.5 and 1.4 are random phases and U_z^e was chosen to satisfy Ampère's law at time $t = 0$. Other parameters include $m_i/m_e = 25$ and the artificial collision rate $\nu = 1$. The species-dependent parameters used in the definition of the Hermite functions are set as follows: $\alpha_\beta^e = \sqrt{2}v_{T\beta}^e = 0.25$, $u_\beta^e = 0$ and $\alpha_\beta^i = \sqrt{2}v_{T\beta}^e/\sqrt{m_i/m_e} = 0.05$, $u_\beta^i = 0$ with $\beta \in \{x, y, z\}$.

Similarly to the previous numerical tests, we study the seven methods summarized in Table 1. As a qualitative measure of the performances of the proposed methods, we report in Fig. 8 the plasma current along the z -axis at the final simulation time $t = 1000$. All runs with $N_{DG} = 2$ (third and fourth columns) show visually indistinguishable solutions. We note that further increasing the temporal, spatial, or velocity resolution does not lead to visible changes in the results (more refined runs are not reported here). All runs with $N_{DG} = 1$ (first and second columns), except for the MRKU0 method, produce qualitatively similar plots, but slightly smeared due to the spatial discretization error. The MRKU0 method with $N_{DG} = 1$ (sixth row, first and second columns) produce results polluted by high amplitude oscillations, which make the results unreliable. The nature of those oscillations could be related to the unphysical modes which were present in the X-mode test in the previous section, see the bottom left panel of Fig. 7.

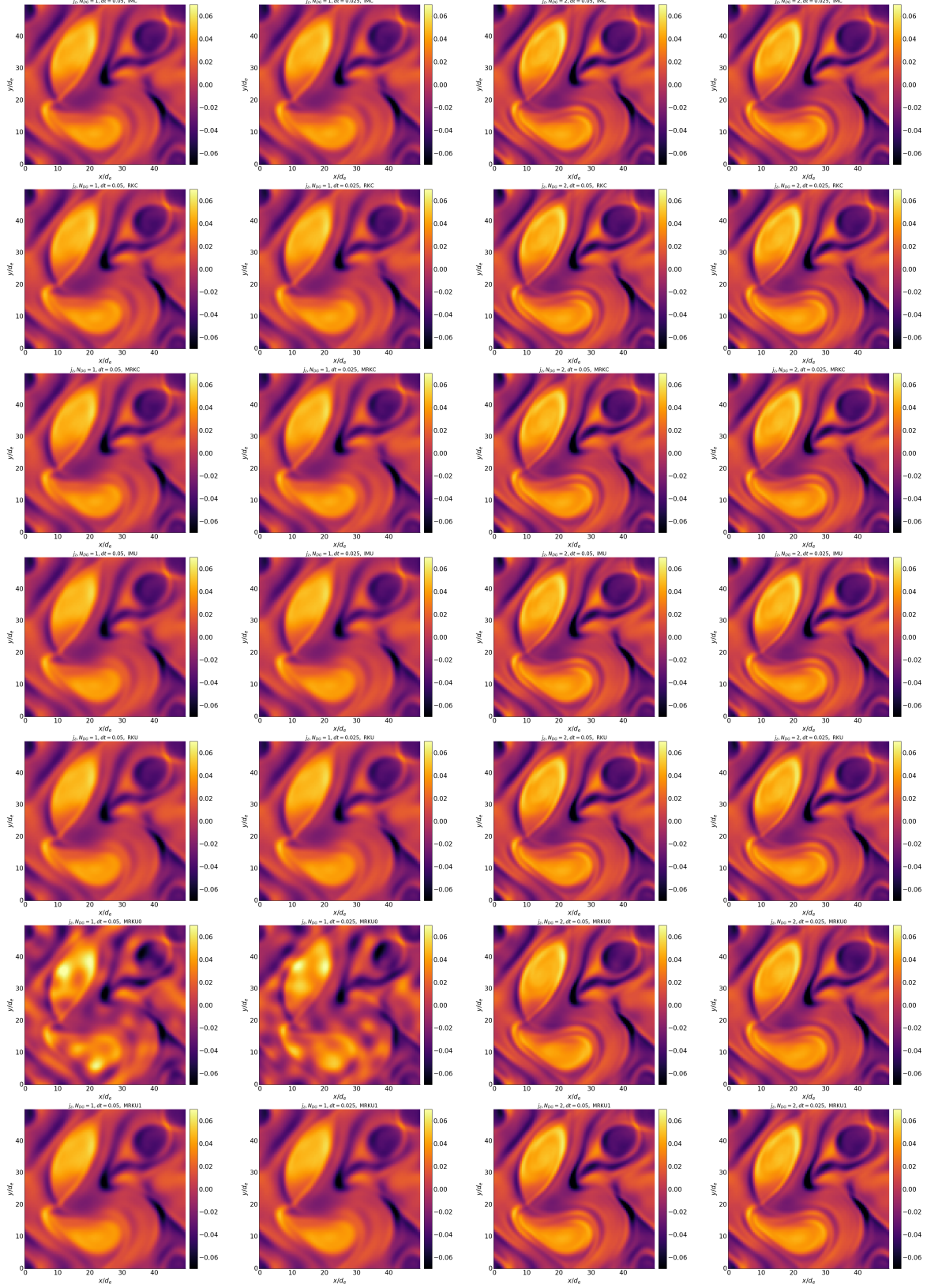


Figure 8: Orszag-Tang vortex benchmark: out of plane current at $t = 1000$ for IMC (first row), RKC (second row), MRKC (third row), IMU (fourth row), RKU (fifth row), MRKU0 (sixth row), MRKU1 (seventh row) with $N_{DG} = 1$ (first and second column), $N_{DG} = 2$ (third and fourth column), $\Delta t = 0.05$ (first and third column), $\Delta t = 0.025$ (second and fourth column).

Concerning the energy conservation in the Orszag-Tang vortex test, we distinguish the case of central fluxes in the spatial approximation of Maxwell's equations (Fig. 9) and upwind fluxes (Fig. 10). The results for central fluxes are similar to the results obtained with the same numerical methods in the whistler instability test in Fig. 4. In the left panel of Fig. 9, the error in the conservation of energy for the IMC scheme is shown: energy is conserved up to the nonlinear solver tolerance. The middle panel illustrates the performances of the RKC scheme, where the error in the energy conservation depends on the accuracy of the temporal discretization (the error is independent on N_{DG} and scales as the Runge-Kutta order producing a reduction of the error by a factor of $\sim 8 = 2^3$ shown with the two sided black arrow). The right panel shows the results obtained with the MRKC scheme, which confirm that the conservation of energy is satisfied to machine precision.

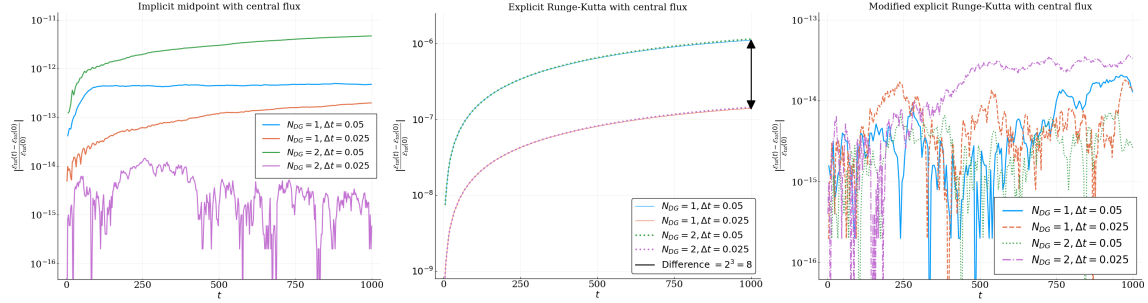


Figure 9: Orszag-Tang vortex benchmark: time evolution of relative error in energy conservation for IMC (left), RKC (middle), and MRKC (right) for different spatial and temporal resolution.

The results for the methods based on upwind fluxes are shown in Fig. 10, and are similar to the ones obtained in the whistler instability test in Fig. 5. The MRKU0 method (left panel) conserves the energy to machine precision although the plot of the current in Fig. 8 shows unsatisfactory results (at least for $N_{DG} = 1$). All other upwind methods, i.e., IMU, RKU, MRKU1 dissipate energy. The middle panel of Fig. 10 has results with $N_{DG} = 1$ and the right panel has $N_{DG} = 2$. As before, the effect of the temporal discretization is small compared to the spatial discretization error for $N_{DG} = 1$ and the curves associated with different methods and different Δt coincide. For $N_{DG} = 2$ (right panel), the energy error in some of the methods differ for $t < 400$. In general, RKU has an energy error that is one to two orders of magnitude larger than that of IMU and MRKU1, showing that in this case the correction for upwind based Runge-Kutta methods is important. The correct third order scaling of RKU is also recovered, as shown by comparing the curves with $\Delta t = 0.05$ and $\Delta t = 0.025$. The energy errors for IMU and MRKU1 essentially coincide, irrespective of Δt . For $t > 400$, the energy error becomes dominated by the spatial discretization error and all the curves essentially overlap (cf. Fig. 5).

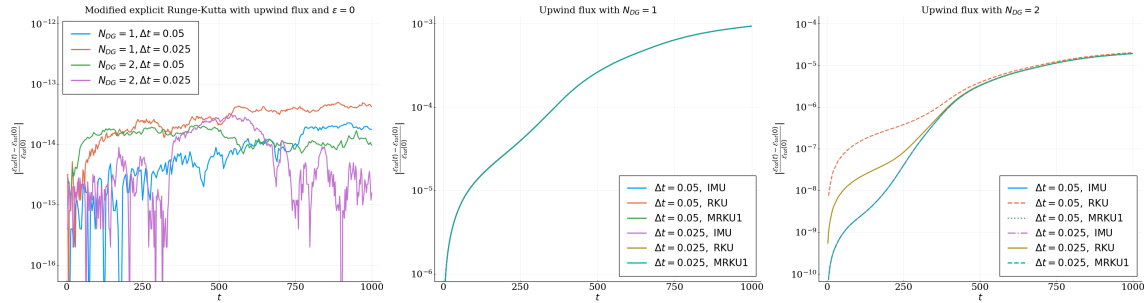


Figure 10: Orszag-Tang vortex benchmark: time evolution of relative error in energy conservation for MRKU0 (left), IMU, RKU, MRKU1 with $N_{DG} = 1$ (middle), and IMU, RKU, MRKU1 with $N_{DG} = 2$ (right), for different resolution.

Finally, we look at how the electromagnetic energy $\mathcal{E}_{E,B}$ defined in (32) changes over time for various methods. The evolution of the electromagnetic energy for runs with $N_{DG} = 2$ looks essentially identical

for all methods and time steps (not shown here). Therefore, we use a run with $N_{DG} = 2$, $\Delta t = 0.025$ and the IMC method as a reference in the following results. The left panel in Fig. 11 shows the evolution of $\mathcal{E}_{E,B}$ for runs with central flux and $N_{DG} = 1$. One can see that the central flux based methods reproduce the correct dynamics of the electromagnetic energy (as seen by comparing them against the more resolved reference solution). At the same time, IMU, RKU, and MRKU1 with $N_{DG} = 1$ consistently dissipate electromagnetic energy for different time step sizes, as shown in the middle panel in Fig. 11. The right panel in Fig. 11 shows the evolution of $\mathcal{E}_{E,B}$ for the MRKU0 method with $N_{DG} = 1$. This method conserves the total energy but it overestimates the energy stored in the electromagnetic field. This additional energy is probably related to the unphysical small scale fluctuations observed in the current plots in Fig. 8.

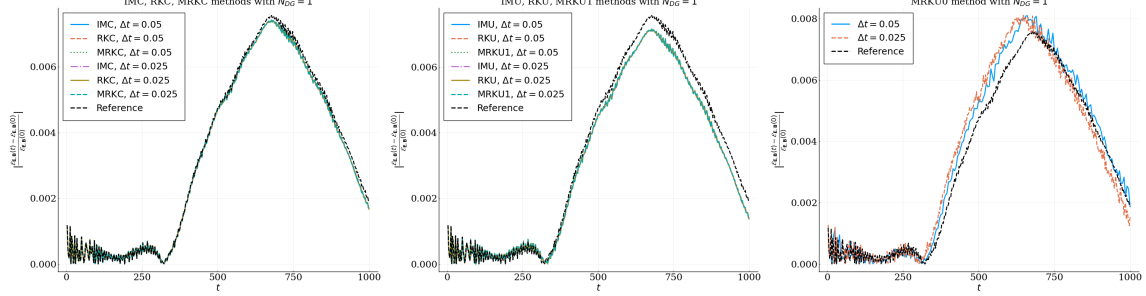


Figure 11: Orszag-Tang vortex benchmark: time evolution of relative change in electromagnetic energy $\mathcal{E}_{E,B}$ for $N_{DG} = 1$ and IMC, RKC, MRKC (left), IMU, RKU, MRKU1 (middle), MRKU0 (right), for different Δt against reference solution (IMC with $N_{DG} = 2$, $\Delta t = 0.025$).

7.4 Notes on momentum conservation and positivity

The total momentum is a conserved quantity of the Vlasov-Maxwell system at the continuum and for periodic boundary conditions. However, as shown in [29, Theorem 5.2], the Hermite-DG discretization of the problem does not exactly conserve the discrete total momentum. If the solution fields are sufficiently regular, the error in the conservation of the discrete momentum decreases according to the order of the semi-discrete approximation. In this section we show that, once we introduce a discretization in time, such violation of the momentum conservation is independent of the temporal integrator. We consider the discrete total momentum defined as

$$P = \sqrt{P_x^2 + P_y^2 + P_z^2},$$

where

$$P_x = \sum_{I,l} \left(\int_I |\varphi^{I,l}(\mathbf{x})|^2 d\mathbf{x} \right) \left(\left(\frac{\omega_{ce}}{\omega_{pe}} \right)^2 (E_y^{I,l} B_z^{I,l} - B_y^{I,l} E_z^{I,l}) + \sum_s m^s \alpha_x^s \alpha_y^s \alpha_z^s \left(u_x^s C_{0,0,0}^{s,I,l} + \frac{\alpha_x^s}{\sqrt{2}} C_{1,0,0}^{s,I,l} \right) \right),$$

and P_y and P_z are defined similarly. Figure 12 shows the evolution of the discrete total momentum (the initial momentum is zero) for different test cases and temporal integrators. The left panel shows results for the whistler instability test with $N_{DG} = 1$ and $\Delta t = 0.01$, where the error in the explicit methods is of the order of machine precision and in the implicit method is of the order of the tolerance of the nonlinear solver. The middle panel shows results for the high frequency electromagnetic waves test, where the error is essentially independent of the time integration strategy. The right panel shows results for the OT test with $N_{DG} = 2$ and $\Delta t = 0.025$, where the error is also independent of the time integration strategy.

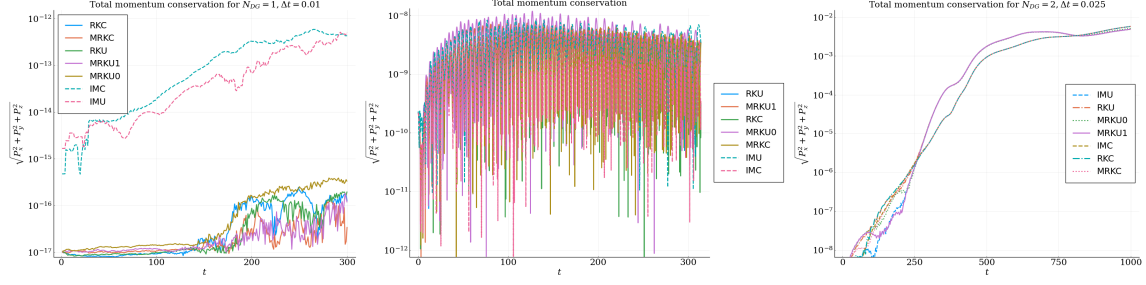


Figure 12: Time evolution of total momentum for different time integration strategies for: whistler instability test with $N_{DG} = 1$ and $\Delta t = 0.01$ (left); high frequency electromagnetic waves test (middle); OT test with $N_{DG} = 2$ and $\Delta t = 0.025$ (right).

Another important issue, common to spectral methods, is that the positivity of the distribution function is not guaranteed in the method considered. As an example, in the most difficult test studied in the paper (the OT test), the reconstructed distribution function has regions with negative values for sufficiently large velocities, whose magnitude at late times and at $v > 3v_T$ (where v_T is the thermal velocity) is $\sim 2\%$ of the (positive) peak value. The error associated with the lack of positivity of the distribution function is fairly insensitive to the time discretization strategy.

We note that the algorithm presented here can be considered as a reduced kinetic model where the distribution function is typically represented with only a few polynomials per velocity direction (4 in the OT test). The negativity of the reconstructed distribution function at some values of the velocity has no obvious consequences for the algorithm, as long as it does not introduce significant errors in the first N_v moments of the distribution. Additionally, adding more Hermite moments mitigates the positivity problem effectively.

8 Conclusions

We presented the analysis of the conservation properties of the fully-discrete numerical approximation of the Vlasov-Maxwell equations provided by the spectral-discontinuous Galerkin method proposed in [29]. Here the velocity space of the Vlasov equation is expanded in asymmetrically weighted Hermite functions while the spatial part of the Vlasov equation and Maxwell's equations are discretized with the DG method. The number of particles is conserved in the semi-discrete formulation of the method, while the total energy is conserved if Maxwell's equations are discretized with central fluxes and dissipates when upwind fluxes are used. Such conservation and dissipation properties are maintained at the fully discrete level by (implicit) Gauss-Legendre temporal integrators but not by explicit Runge-Kutta schemes. Hence, we have adopted *modified* RK schemes, known as incremental direction techniques (IDT) [4] and relaxation Runge-Kutta methods (RRK) [27], and analyzed them in the context of the Hermite-DG discretization of the Vlasov-Maxwell equations. These are explicit Runge-Kutta methods that maintain the properties of the semi-discrete system by applying a correction step to the regular Runge-Kutta algorithm. The idea behind the method is to tie the correction step to the conservation of a particular quantity (the total energy in this case).

For upwind fluxes in Maxwell's equations, which provide numerical energy dissipation associated with the DG jumps at the cell interfaces, one might be tempted to apply the Runge-Kutta correction step in a way that forces exact conservation of the total energy (i.e. the conservation property of the system at the continuum level and not at the semi-discrete level). Indeed, we have tested this possibility numerically [Eq. (55) with $\varepsilon = 0$, scheme MRKU0 in Table 1] against an approach where the correction step is chosen to preserve the upwind energy dissipation [Eq. (55) with $\varepsilon = 1$, scheme MRKU1 in Table 1; this is equivalent to enforcing energy conservation at the semi-discrete level such that to preserve upwind energy dissipation]. In all our numerical experiments, MRKU0 consistently showed lower accuracy of the overall solution relative to MRKU1 when used in conjunction with linear polynomials ($N_{DG} = 1$) for DG. For instance, in the Orszag-Tang decaying turbulence test, Fig. 8, one can see spurious oscillations in the MRKU0 solution (sixth row, first two columns) that are not present

in any of the other methods. These oscillations disappear when one increases the order of the spatial discretization ($N_{DG} = 2$, sixth row, third and fourth columns in Fig. 8). These results suggest that preserving the properties of the semi-discrete formulation of the method at the fully-discrete level and controlling the numerical dissipation through the accuracy of the spatial discretization might provide a better algorithm when upwind fluxes are used in Maxwell's equations. For central fluxes, the total energy is a conserved quantity of the evolution problem ensuing from the Hermite-DG discretization since the terms associated with the jumps at cell interfaces disappear. In this case, the modified RK scheme ensures energy conservation at the fully-discrete level.

In closing, we note that explicit time integrators that can conserve energy at the discrete level, such as those discussed in this paper, are very important for plasma physics applications since these methods are much less computationally expensive than the implicit time integrators that also typically can conserve energy. Depending on the application, implicit methods might still be preferable for their overall better numerical stability. Future work might seek the development of energy-conserving semi-implicit methods that combine the advantages of the two classes of schemes and achieve energy conservation in the discrete, while relaxing the computational cost of fully-implicit schemes (as done recently in the area of Particle-In-Cell methods [31]).

Declarations

Funding. The work of GLD, OK, GM was supported by the Laboratory Directed Research and Development - Exploratory and Research (LDRD-ER) Program of Los Alamos National Laboratory under project number 20170207ER. Los Alamos National Laboratory is operated by Triad National Security, LLC, for the National Nuclear Security Administration of U.S. Department of Energy (Contract No. 89233218CNA000001). Computational resources for the SPS-DG simulations were provided by the Los Alamos National Laboratory Institutional Computing Program.

VR's contributions were supported by DOE grant DE-SC0019315.

Data availability statement. Data sharing not applicable to this article as no datasets were generated or analysed during the current study.

References

- [1] J. A. Bittencourt. *Fundamentals of Plasma Physics*. Springer-Verlag New York, 2004.
- [2] P. Bogacki and L. F. Shampine. A 3 (2) pair of Runge-Kutta formulas. *Applied Mathematics Letters*, 2(4):321–325, 1989.
- [3] T. J. M. Boyd and J. J. Sanderson. *The Physics of Plasmas*. Cambridge University Press, 2003.
- [4] M. Calvo, D. Hernández-Abreu, J. Montijano, and L. Rández. On the preservation of invariants by explicit Runge–Kutta methods. *SIAM Journal on Scientific Computing*, 28(3):868–885, 2006.
- [5] M. Campos Pinto, K. Kormann, and E. Sonnendrücker. Variational framework for structure-preserving electromagnetic particle-in-cell methods. *J. Sci. Comput.*, 91(2):Paper No. 46, 39, 2022.
- [6] C. Z. Cheng and G. Knorr. The integration of the Vlasov equation in configuration space. *Journal of Computational Physics*, 22(3):330 – 351, 1976.
- [7] G. J. Cooper. Stability of Runge-Kutta methods for trajectory problems. *IMA J. Numer. Anal.*, 7(1):1–13, 1987.
- [8] K. Dekker and J. G. Verwer. *Stability of Runge-Kutta methods for stiff nonlinear differential equations*, volume 2 of *CWI Monographs*. North-Holland Publishing Co., Amsterdam, 1984.
- [9] N. Del Buono and C. Mastroserio. Explicit methods based on a class of four stage fourth order Runge–Kutta methods for preserving quadratic laws. *Journal of Computational and Applied Mathematics*, 140(1):231–243, 2002. Int. Congress on Computational and Applied Mathematics 2000.

- [10] G. L. Delzanno. Multi-dimensional, fully-implicit, spectral method for the Vlasov-Maxwell equations with exact conservation laws in discrete form. *Journal of Computational Physics*, 301:338–356, 2015.
- [11] James W. Eastwood. The virtual particle electromagnetic particle-mesh method. *Computer Physics Communications*, 64(2):252–266, 1991.
- [12] E. Eich-Soellner and C. Führer. *Numerical methods in multibody dynamics*. European Consortium for Mathematics in Industry. B. G. Teubner, Stuttgart, 1998.
- [13] D. Funaro. *Polynomial approximation of differential equations*, volume 8. Springer Science & Business Media, 2008.
- [14] S. P. Gary. *Theory of space plasma microinstabilities*. Cambridge University Press, 2005.
- [15] R. T. Glassey. *The Cauchy problem in kinetic theory*, volume 52. SIAM, 1996.
- [16] R. J. Goldston and P. H. Rutherford. *Introduction to Plasma Physics*. CRC Press, 1995.
- [17] H. Grad. On the kinetic theory of rarefied gases. *Communications on Pure and Applied Mathematics*, 2(4):331–407, 1949.
- [18] V. Grimm and G. R. W. Quispel. Geometric integration methods that preserve Lyapunov functions. *BIT*, 45(4):709–723, 2005.
- [19] E. Hairer, C. Lubich, and G. Wanner. *Geometric numerical integration. Structure-preserving algorithms for ordinary differential equations*, volume 31 of *Springer Series in Computational Mathematics*. Springer, Heidelberg, 2010.
- [20] E. Hairer, S. P. Nørsett, and G. Wanner. *Solving ordinary differential equations I. Nonstiff problems*, volume 8 of *Springer Series in Computational Mathematics*. Springer-Verlag, Berlin, second edition, 1993.
- [21] E. Hairer and G. Wanner. *Solving ordinary differential equations II. Stiff and differential-algebraic problems*, volume 14 of *Springer Series in Computational Mathematics*. Springer-Verlag, Berlin, 2010.
- [22] Y. He, Y. Sun, J. Liu, and H. Qin. Volume-preserving algorithms for charged particle dynamics. *Journal of Computational Physics*, 281:135–147, 2015.
- [23] J. S. Hesthaven and T. Warburton. High-order nodal discontinuous Galerkin methods for the Maxwell eigenvalue problem. *Philosophical Transactions of the Royal Society of London. Series A: Mathematical, Physical and Engineering Sciences*, 362(1816):493–524, 2004.
- [24] A. Iserles. *A first course in the numerical analysis of differential equations*. Cambridge Texts in Applied Mathematics. Cambridge University Press, Cambridge, 1996.
- [25] G. Joyce, G. Knorr, and H. K. Meier. Numerical integration methods of the Vlasov equation. *Journal of Computational Physics*, 8(1):53–63, 1971.
- [26] J. Juno, A. Hakim, J. TenBarge, E. Shi, and W. Dorland. Discontinuous Galerkin algorithms for fully kinetic plasmas. *Journal of Computational Physics*, 353:110–147, 2018.
- [27] D. I. Ketcheson. Relaxation Runge-Kutta methods: conservation and stability for inner-product norms. *SIAM J. Numer. Anal.*, 57(6):2850–2870, 2019.
- [28] K. Kormann and E. Sonnendrücker. Energy-conserving time propagation for a structure-preserving particle-in-cell vlasov-maxwell solver. *Journal of Computational Physics*, 425:109890, 2021.
- [29] O. Koshkarov, G. Manzini, G. L. Delzanno, C. Pagliantini, and V. Roytershteyn. The multi-dimensional Hermite-discontinuous Galerkin method for the Vlasov-Maxwell equations. *Computer Physics Communications*, 264:107866, 2021.

- [30] M. Kraus, K. Kormann, P. J. Morrison, and E. Sonnendrücker. Gempic: geometric electromagnetic particle-in-cell methods. *Journal of Plasma Physics*, 83(4):905830401, 2017.
- [31] G. Lapenta. Exactly energy conserving semi-implicit particle in cell formulation. *Journal of Computational Physics*, 334:349–366, 2017.
- [32] H. R. Lewis. Energy-conserving numerical approximations for vlasov plasmas. *Journal of Computational Physics*, 6(1):136–141, 1970.
- [33] H. R. Lewis. Variational algorithms for numerical simulation of collisionless plasma with point particles including electromagnetic interactions. *Journal of Computational Physics*, 10(3):400–419, 1972.
- [34] G. Manzini, G. L. Delzanno, J. Vencels, and S. Markidis. A Legendre-Fourier spectral method with exact conservation laws for the Vlasov-Poisson system. *Journal of Computational Physics*, 317:82–107, 2016.
- [35] S. A. Orszag and C.-M. Tang. Small-scale structure of two-dimensional magnetohydrodynamic turbulence. *Journal of Fluid Mechanics*, 90(1):129–143, 1979.
- [36] T. N. Parashar, M. A. Shay, P. A. Cassak, and W. H. Matthaeus. Kinetic dissipation and anisotropic heating in a turbulent collisionless plasma. *Physics of Plasmas*, 16(3):032310, 2009.
- [37] D. Sármany, M. A. Botchev, and J. J. W. van der Vegt. Dispersion and dissipation error in high-order Runge-Kutta discontinuous Galerkin discretisations of the Maxwell equations. *Journal of Scientific Computing*, 33(1):47–74, 2007.
- [38] J. W. Schumer and J. P. Holloway. Vlasov simulations using velocity-scaled Hermite representations. *J. Comput. Phys.*, 144(2):626–661, 1998.
- [39] M. Tao. Explicit high-order symplectic integrators for charged particles in general electromagnetic fields. *Journal of Computational Physics*, 327:245–251, 2016.
- [40] M. Wan, W.H. Matthaeus, H. Karimabadi, V. Roytershteyn, M. Shay, P. Wu, W. Daughton, B. Loring, and S.C. Chapman. Intermittent Dissipation at Kinetic Scales in Collisionless Plasma Turbulence. *Physical Review Letters*, 109(19):195001, nov 2012.